PCCP
Physical Chemistry Chemical Physics

Accepted Manuscript

This article can be cited before page numbers have been issued, to do this please use: D. Matyushov, *Phys. Chem. Chem. Phys.*, 2023, DOI: 10.1039/D2CP06072H.

ROYAL SOCIETY OF CHEMISTRY

rsc.li/pccp

View Article Online
DOI: 10.1039/D2CP06072H

PCCP

ARTICLE TYPE

Cite this: DOI: 00.0000/xxxxxxxxxx

Reorganization Energy of Electron Transfer

Dmitry V. Matyushov*[a]

Received Date
Accepted Date

DOI: 00.0000/xxxxxxxxxx

The theory of electron transfer reactions establishes the conceptual foundation for redox solution chemistry, electrochemistry, and bioenergetics. Electron and proton transfer across the cellular membrane provide all energy of life gained through natural photosynthesis and mitochondrial respiration. Rates of biological charge transfer set kinetic bottlenecks for biological energy storage. The main system-specific parameter determining the activation barrier for a single electron-transfer hop is the reorganization energy of the medium. Both harvesting of light energy in natural and artificial photosynthesis and efficient electron transport in biological energy chains require reduction of the reorganization energy to allow fast transitions. This review article discusses mechanisms by which small values of the reorganization energy are achieved in protein electron transfer and how similar mechanisms can operate in other media, such as nonpolar and ionic liquids. One of the major mechanisms of reorganization energy reduction is through non-Gibbsian (nonergodic) sampling of the medium configurations on the reaction time. A number of alternative mechanisms, such as electrowetting of active sites of proteins, give rise to non-parabolic free energy surfaces of electron transfer. These mechanisms, and nonequilibrium population of donor-acceptor vibrations, lead to a universal phenomenology of separation between the Stokes-shift and variance reorganization energies of electron transfer.

1 Introduction

This article is about the reorganization energy of electron transfer. It has become a central parameter in studies of electron transfer within and between molecules since the development of the theory of electron-transfer reactions in solutions by Marcus.[1] A number of alternative definitions of this parameter are discussed below. We start with the definition in terms of small thermal fluctuations around equilibria, thus avoiding highly nonequilibrium states implicit to some other definitions.

Electron transfer represents the process of a tunneling transition of an electron between two localized states on the donor and acceptor molecules or molecular groups. The reorganization energy λ is required to specify the activation barrier to reach the tunneling configuration. It is best defined[2] through the variance of the reaction coordinate X (in units of energy) describing the progression of the reaction from the reactant state (electron on the donor) to the product state (electron on the acceptor)

$$\lambda = \tfrac{1}{2}\beta\langle(\delta X)^2\rangle. \qquad (1)$$

Here, $\beta = (k_B T)^{-1}$ denotes the inverse thermal energy and angular brackets refer to a statistical average over the system configurations producing fluctuations of the stochastic variable X, with $\delta X = X - \langle X\rangle$ denoting the fluctuation from the average value $\langle X\rangle$. The reaction coordinate for electron transfer is distinct from many other chemical reactions where some geometrical parameters, such as the distance between the reactants and products, is used to monitor the reaction progress.[3] Instead, X carries the units of energy and is defined as the difference in energies of the transferring electron in the final (at the acceptor) and initial (at the donor) states. If the electronic energy is E_2 on the acceptor and E_1 on the donor, electron tunneling requires equality between E_1 and E_2 dubbed as the resonance condition. The reaction coordinate was defined by Lax[4] and Warshel[5] as the energy gap, the difference, between the acceptor and donor energies

$$X = E_2 - E_1. \qquad (2)$$

The resonance condition at which electron tunnels and the reaction reaches the top of the activation barrier is specified by $X = 0$.

Given that the exact equality between equilibrium values of E_1 and E_2 is nearly impossible, thermal fluctuations of the energy gap are required to establish the tunneling configuration. The reorganization energy in eqn (1) thus quantifies the breadth of such fluctuations, i.e., the spread of the energy-gap distribution. It is important to stress that the energy-gap variance in eqn (1) is calculated from the statistics of small deviations δX from the stationary value $\langle X\rangle$. This statistics is not necessarily sampled from a canonical Gibbsian ensemble and can be produced from more general ensembles, including those with imposed constraints, as

[a] School of Molecular Sciences and Department of Physics, Arizona State University, PO Box 871504, Tempe, Arizona 85287-1504, USA; E-mail: dmitrym@asu.edu

View Article Online
DOI: 10.1039/D2CP06072H

discussed below.

This Perspective reports recent results for charge transport in complex molecular systems, such as proteins, ionic liquids, and nonpolar liquids. It connects new challenges posed by these media with fundamental concepts established when the theory of molecular electron transfer was envisioned.[6–8] Classical theories of electron transfer, while providing firm conceptual background, also predict the existence of significant energetic bottlenecks to efficient charge transport in natural and artificial molecular systems. How some of these limitations have been lifted by nature's creativity is a fascinating ongoing inquiry accomplished by laboratory measurements and, increasingly, by computer simulations. Condensing these recent advances into a framework of generic formal theories is one of the goals pursued by this report.

Light harvesting is an important natural[9, 10] and technological[11] application of electron transfer in molecular systems. Absorption of light lifts the energy of the molecule by the photon energy $h\nu$ to allow reactions that are thermodynamically forbidden.[12] In molecules, the separation of charge between the donor and acceptor parts of the donor-acceptor complex occurs by absorbing the light photon either by a separate antenna system or directly by the donor molecule[13] thus producing the photoexcited electron donor D^*. Charge separation (CS) competes with charge recombination (CR) according to the following simplified kinetic scheme

$$D-A \xrightarrow{h\nu} D^*-A \xrightarrow{k_{CS}} D^+-A^- \xrightarrow{k_{CR}} D-A. \qquad (3)$$

To utilize the photon energy for subsequent charge transport, the rate constant of charge separation k_{CS} must be much greater than the rate of charge recombination k_{CR} to the ground state D–A.[14] The efficiency of charge separation is specified by the quantum yield Y equal to the ratio of the number of charge-separated products to the number of absorbed photons: $Y \simeq 0.95$ for primary charge separation in bacterial photosynthesis.[9, 15, 16]

From the energy diagram shown in Fig. 1, it is clear that the free energies of the CS and CR reactions ΔG_a, $a = \mathrm{CS}, \mathrm{CR}$ add up to satisfy the energy conservation

$$\sum_a |\Delta G_a| = h\nu. \qquad (4)$$

There is another restriction, imposed by kinetics, which turns out to be critical for the values of reorganization energies of the corresponding reactions. To allow the fastest CS, the reaction driving force (negative of the reaction free energy) should be equal to the reorganization energy λ_{CS}. The reaction free energy of CR is still negative and, to avoid fast backward reaction, CR needs to be in the Marcus inverted region[6] (see below for definition). Combining CS and CR transitions, one arrives at the second constraint imposed on the reaction free energies involved

$$\sum_a |\Delta G_a| > \sum_a \lambda_a. \qquad (5)$$

Assuming $\lambda_{CS} \simeq \lambda_{CR} \simeq \lambda$, an energetic constraint on the reorganization energy value follows

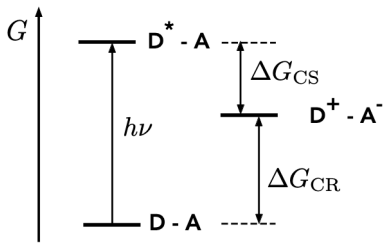

Fig. 1 Energy diagram of charge separation and charge recombination reaction in natural and artificial light harvesting. Shown are the free-energy levels of the reaction steps in eqn (1) and the reaction free energies ΔG_a $(a = \mathrm{CS}, \mathrm{CR})$.

$$\lambda < \tfrac{1}{2} h\nu. \qquad (6)$$

The reorganization energy has to be sufficiently low to allow light harvesting with high quantum yield.

Natural bacterial photosynthesis often operates on the red side of the visible spectrum with $h\nu \simeq 1.8$ eV for chlorophyll *a* pigments in oxygenic species.[16] The reaction center of much studied[9] *Rhodobacter sphaeroides* anaerobic purple bacterium absorbs $h\nu \simeq 1.4$ eV photon by its primary pair of two sandwiched bacteriochlorophyll pigments (lower edge of the exciton band). Equation (6) requires $\lambda < 0.7$ eV. It was indeed found that first two charge-separation steps of natural photosynthesis occur as nearly activationless transitions with the reorganization energies[17–19] of $\lambda_{CS} \simeq 0.35$ eV for the primary charge separation and $\lambda \simeq 0.5$ eV[20] for the second step. There is just a slight mismatch between λ_{CS} and $\Delta G_{CS} \simeq -0.25$ eV. Quoting from Marcus:[21] "It has been suggested that the small λ (0.25 eV) and the resulting inverted region effect play a significant role in providing this essential condition for the effectiveness of the photosynthetic reaction center."

Small values of reorganization energy found for primary charge separation in natural photosynthesis satisfy the energy requirement for high quantum yield (eqn (6)), but pose the mechanistic question of how such low values are achieved by the protein medium. While dried protein powders are often viewed as nonpolar media since they show low values of the bulk dielectric constant, proteins in aqueous solutions are decorated by large numbers of ionized surface residues.[22] Thermally induced elastic deformations of the protein shift surface charges thus producing significant electrostatic fluctuations[23] more consistent with highly polar than nonpolar media (see below). In addition, active sites of many redox-active proteins are located in sufficient proximity to highly polar water to allow a substantial water component in the medium reorganization energy. Nevertheless, it appears that low values of the reorganization energy are universally achieved in active sites of redox-active proteins. Reorganization energies in the range $0.5 - 0.7$ eV, or lower, are required to explain electron transport in biological energy chains.[24] Electron hopping in chains of biological redox cofactors often occurs with near-zero reaction free energy,[25] making the reorganization energy the main parameter affecting the activation barrier.

View Article Online
DOI: 10.1039/D2CP06072H

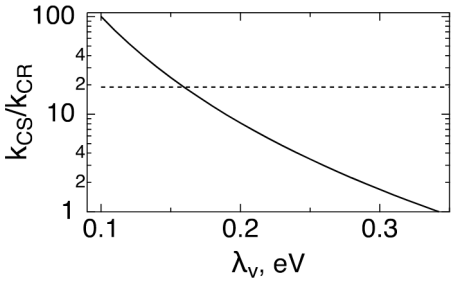

Fig. 2 k_{CS}/k_{CR} vs λ_v for the reaction center of *Rhodobacter sphaeroides* anaerobic purple bacterium. The parameters for the CS reaction are: $\Delta G_{CS} = -0.25$ eV,[9] $\lambda = 0.35$ eV,[17, 18] $\omega_v = 1300$ cm^{-1}. The dashed line is based on the experimental quantum yield $Y \simeq 0.95$; the crossing of theoretical solid line with the experimental dashed line occurs at $\lambda_v \simeq 0.15$ eV. The theoretical line is from the Bixon-Jortner equation (eqn (57)) assuming that the electronic coupling is conserved between CS and CR.

The requirement of a low medium reorganization energy also extends to the internal reorganization of vibrational modes of the donor and acceptor.[26, 27] As we discuss below, intramolecular vibrations increase the rate of charge recombination in the Marcus inverted region ($-\Delta G > \lambda$) thus lowering the quantum yield. The effect of intramolecular vibrations on the quantum yield is illustrated in Fig. 2 where the ratio of $k_{CS}/k_{CR} = Y/(1-Y)$ is shown vs the vibrational reorganization energy λ_v (see below) for primary charge transfer in the reaction center of *Rhodobacter sphaeroides*. The outcome from the experimental quantum yield is shown by the horizontal dashed line, which sets $\lambda_v < 0.15$ eV. This low value, which requires significant rigidity of the protein active site, is indeed achieved for many redox-active proteins. Estimated values range from 0.05-0.09 eV for Fe-porphins[28] to 0.10-0.14 eV for Zn porphyrins[29] and 0.1 eV for azurins.[30]

The case of protein electron transfer is significant given how much can be learned from natural systems about the principles of optimizing light harvesting and charge transport in mesoscopic molecular systems. The problem is obviously important on its own since protein electron transfer is the basis of energetics of life. The range of applications of electron transfer is still much broader, embracing solar energy harvesting,[10, 11] photocatalysis,[12] electrochemistry,[31] and bioenergetics,[25] to name just a few. This Perspective article cannot even touch on most of these active research areas. The main focus here is on basic parameters affecting the reaction activation energy and fundamental principles behind electron transport in molecules. Fundamental ingredients of the standard theory are reviewed with an eye on their potential modifications and extensions as the scope of research effort is broadened to many new materials for charge-transfer applications. One naturally wonders if new properties of novel materials, distinct from polar molecular solvents envisioned when the theory was originated,[1] can bring new parameters to tune in order to achieve higher efficiency of charge separation for energy storage and charge transport. One of the major findings of studies of protein electron transfer is that the relaxation time, in addition to the Gibbs energy, can be efficiently used to modify the reaction activation barrier.[32]

A few words about notations adopted here. Gibbs free energy G is relevant for experiments performed at constant-pressure conditions, and those are used in the energy balance diagram in Fig. 1. In contrast, the Gibbsian canonical ensemble defines the Helmholtz free energy F corresponding to constant volume. Statistical mechanics, operating with canonical ensembles, produce Helmholtz free energies entering our theoretical arguments presented below. For all practical purposes, the Gibbs and Helmholtz free energies are mostly indistinguishable for reactions in condensed media.

2 Crossing parabolas

A great success of Marcus theory is the ability to map a very complex process of quantum tunneling in a condensed medium to a simple graphical representation in terms of two crossing parabolas. The parabolas themselves are partial free energies or potentials of mean force specifying the reversible work invested to arrive to all possible configurations consistent with a given value X of the donor-acceptor energy gap. Given that many configurations of the system must be involved, one anticipates that the partial free energy $F_i(X)$ contains both energy, $U_i(X)$, and entropy, $S_i(X)$, contributions

$$F_i(X) = U_i(X) - TS_i(X). \tag{7}$$

Here, from standard rules of thermodynamics, one has

$$S_i(X) = -(\partial F_i/\partial T)_V\,. \tag{8}$$

Mathematically, the free energy surfaces $F_i(X)$ are derived from the canonical Gibbsian ensemble by tracing out all possible configurations of the medium and of the donor-acceptor complex while keeping the energy gap constant. This is achieved by putting the delta-function in the definition of the partial partition function as follows

$$e^{-\beta F_i(X)} \propto \int d\Gamma \delta\left(X - E_2(\Gamma) + E_1(\Gamma)\right) e^{-\beta H_i}. \tag{9}$$

Here, $\exp[-\beta H_i]$ is the Boltzmann factor of the Gibbsian ensemble specified by the Hamiltonian H_i in two electron-transfer states $i = 1, 2$ and Γ denotes the entire manifold of all possible configurations of the system (the phase space). The energies E_i are eigenvalues of the donor-acceptor quantum subsystem and the rest of the Hamiltonian $H_i = E_i + H_b$ is not affected by the electronic state.

The energies $E_i(\Gamma)$ in eqn (9) are taken at the same configuration of the atoms and molecules in the system. This requirement constitutes the Franck-Condon principle stating that electronic transitions occur so fast that nuclei of the system are not capable of changing their positions on that very short time. Therefore, the energy gap X is also called the "vertical" energy gap to stress that the nuclear coordinates, usually plotted on the horizontal axis, remain unchanged during the transition.

The constrained partition functions in eqn (9) immediately lead to an important linear relation between two free energy surfaces[33, 34]

$$F_2(X) = F_1(X) + X. \tag{10}$$

View Article Online
DOI: 10.1039/D2CP06072H

This result follows from a simple manipulation in the partition function, which effectively implies the law of energy conservation

$$\int d\Gamma \delta\left(X-\Delta E(\Gamma)\right) e^{-\beta H_1} = \int d\Gamma \delta\left(X-\Delta E(\Gamma)\right) e^{\beta X} e^{-\beta H_2}, \quad (11)$$

where $\Delta E(\Gamma) = E_2(\Gamma) - E_1(\Gamma)$.

The linear relation states that one arrives at the final surface $F_2(X)$ by adding the energy difference $X = \Delta E = \Delta H$ to the initial state $F_1(X)$ at any configuration of the system, either at equilibrium or out of equilibrium. This notion connects the problem of electron transfer to spectroscopy of charge-transfer transitions since the energy of the photon $h\nu = X$ can be used to both initiate charge transfer (eqn (3)) and to probe probabilities of different states X through the optical band-shape. Spectroscopy of charge-transfer bands has therefore become a primary tool in investigating charge-transfer reactions.[35]

Given that the energy gap X is the difference of energies, one anticipates that the entropy components of $F_i(X)$ should cancel in $F_2(X) - F_1(X)$ at every X. This expectation is in accordance with the idea of a "vertical" (optical) transition connecting the free energy surfaces. This result also follows from the linear relation between the free energy surfaces. By taking the temperature derivative of both sides of eqn (10), one arrives at the equality between the entropy surfaces for the reactants and products[36]

$$S_2(X) = S_1(X). \quad (12)$$

The inequality between $F_i(X)$ is thus caused by $U_1(X) \neq U_2(X)$ in eqn (7).

The simplest approximation for the free energy surfaces is to adopt the Gaussian statistics of X. This result follows from the statistical central limit theorem if one assumes that many individual molecules contribute to changes of X through their thermal motions. As we discuss below, this approximation is very reasonable when charge-transfer reactions in polar liquids are concerned. The Gaussian statistics of X implies that each $F_i(X)$ can be specified by two statistical moments, the average $X_i = \langle X\rangle_i$ and the variance

$$\sigma_i^2 = \langle(\delta X)^2\rangle_i. \quad (13)$$

The averages $\langle\ldots\rangle_i$ refer to each electron-transfer state separately, $i = 1$ for the initial state and $i = 2$ for the final state.

With the Gaussian prescription for $\exp[-\beta F_i(X)]$, the free energy surfaces become parabolas. One can additionally apply the relation between the variance in eqn (1) and the reorganization energy to define two separate reorganization energies

$$\lambda_i = \tfrac{1}{2}\beta\langle(\delta X)^2\rangle_i. \quad (14)$$

With this assignment, one gets two parabolas

$$F_i(X) = F_{0i} + \frac{(X-X_i)^2}{4\lambda_i}, \quad (15)$$

where F_{0i} are the equilibrium free energies such that $\Delta F_0 = F_{02} - F_{01}$ is the reaction free energy.

The functions $F_i(X)$ are not Marcus parabolas yet. One needs to additionally impose two exact conditions: the requirement that the free energy surfaces cross at $X = 0$, $F_1(0) = F_2(0)$, and the linear relation from eqn (10). These two relations impose the following constraints on the free energy surfaces

$$\lambda = \lambda_1 = \lambda_2 \quad (16)$$

and

$$\lambda^{\mathrm{St}} = \tfrac{1}{2}(X_1 - X_2), \quad \lambda^{\mathrm{St}} = \lambda. \quad (17)$$

The Stokes-shift reorganization energy[23] λ^{St} is separately defined in terms of the separation of parabolas' minima (Fig. 3). This parameter is closely related to the Stokes shift between absorption and emission maxima in optical spectroscopy, whence the name. We show below that deviations from the equality $\lambda^{\mathrm{St}} = \lambda$, specific to Marcus theory (eqn (17)), are responsible for the catalytic effect of proteins on redox reactions.

The crossing parabolas also specify the reaction free energy as the mean of average values of the reaction coordinate

$$\Delta F_0 = \tfrac{1}{2}(X_1 + X_2). \quad (18)$$

Returning to spectroscopic applications, ΔF_0 can be measured as the crossing point of the absorption and emission charge-transfer bands if they satisfy the mirror symmetry as required for mapping optical charge-transfer bands on the electron-transfer theory.[37]

The fundamental linear relation imposed on the Gaussian statistics of X leaves only one reorganization energy as the parameter relevant for defining the activation barrier of electron transfer. The reorganization energies λ_i define the curvatures of who parabolas, which must be equal to satisfy eqn (10) and, in addition, are equal to λ^{St}. One additional reorganization energy λ^r, originally due to Marcus,[6] can be specified as the free energy required to travel from one parabola's minimum to the position of the second minimum along a single parabolic surface (Fig. 3). The disadvantage of this definition is that it involves a highly nonequilibrium state which does not have to follow the Gaussian statistics always applicable close to parabolas' minima.

From eqn (15), the activation barrier for electron transfer is the vertical distance between the parabolas minima and their crossing

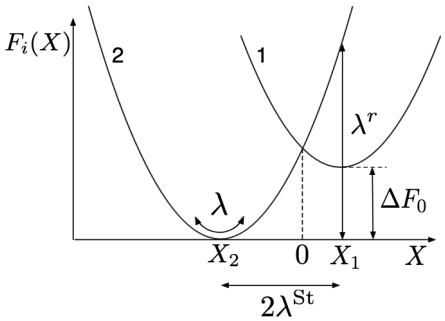

Fig. 3 Free energy surfaces of electron transfer $F_i(X)$. The minima of two parabolas X_i are separated by twice the Stokes-shift reorganization energy $2\lambda^{\mathrm{St}}$. The variance reorganization energy λ (eqn (1)) specifies the curvatures of the parabolas. The change in the free energy required to travel horizontally along each surface the distance $2\lambda^{\mathrm{St}}$ defines the "reaction" reorganization energy λ^r.

View Article Online
DOI: 10.1039/D2CP06072H

point at $X = 0$

$$\Delta F_i^{\dagger} = \frac{X_i^2}{4\lambda} = \frac{(\Delta F_0 \pm \lambda)^2}{4\lambda}. \tag{19}$$

In the second relation, which follows from adding and subtracting eqn (17) and (18), "+" and "−" correspond to $i = 1$ and $i = 2$, respectively. Equation (19) establishes the inverted Marcus parabola representing the reaction rate constant k_r (on the logarithmic scale) plotted vs the driving force $-\Delta F_0$. This energy gap law, confirmed by a number of experimental studies,[14, 38, 39] stipulates that making ΔF_0 more negative is required to move from the normal region for the forward rate $X_1 > 0$ to the highest activationless rate of forward electron transfer at $X_1 = 0$. The rate declines again with further increasing of the driving force $-\Delta F_0$ into the exergonic domain, which specifies the Marcus inverted region $X_1 < 0$.

3 Fluctuation-dissipation relations

The definition of the reorganization energy in eqn (1) involves the product of the energy-gap variance with the inverse thermal energy β. This specific functionality comes from the static limit of the fluctuation-dissipation theorem (FDT) also known as Johnson-Nyquist noise.[40] This theorem states that the variance of a macroscopic variable A should scale linearly with temperature, $\langle(\delta A)^2\rangle \propto T$, $\delta A = A - \langle A\rangle$. When $A = X$, the slope of this linear scaling, which is expected to be little affected by temperature, defines the reorganization energy.

The meaning of the static FDT is easy to appreciate for a harmonic oscillator in contact with the thermostat at temperature T. According to the equipartition theorem, the variance of thermally-induced oscillator displacement δq is $\langle(\delta q)^2\rangle = \chi k_B T$, where the linear susceptibility $\chi = \kappa^{-1}$ is the inverse of the force constant κ. The same susceptibility defines the linear displacement of the oscillator $\Delta q = \chi f_{\text{ext}}$ in response to the external force f_{ext}. The reorganization energy thus becomes a linear susceptibility relating the change in the donor-acceptor energy gap in response to the movement of charge between the donor and acceptor.[41]

The connection between the reorganization energy and susceptibility can be made more explicit by applying Kubo's linear response theory[42, 43] that leads to the FDT in the frequency domain. This formulation[41] specifically considers the time-dependent change of the energy gap $\Delta X(t)$ initiated by the movement of charge between the donor and acceptor at $t = 0$. In Kubo's formalism, the time-dependent response function $\chi(t)$ can be connected to the time correlation function of the variable $X(t)$

$$C_X(t) = \langle \delta X(t)\delta X(0)\rangle, \quad \delta X(t) = X(t) - \langle X\rangle. \tag{20}$$

This connection becomes a linear algebraic relation upon applying the Fourier-Laplace (one-sided Fourier) transform to the time-dependent functions[43]

$$\tilde{\chi}(\omega) = \beta\left[C_X(0) + i\omega\tilde{C}_X(\omega)\right], \tag{21}$$

where tildes are used to denote Fourier-Laplace transformed functions

$$\tilde{C}_X(\omega) = \int_0^{\infty} dt C_X(t) e^{i\omega t}. \tag{22}$$

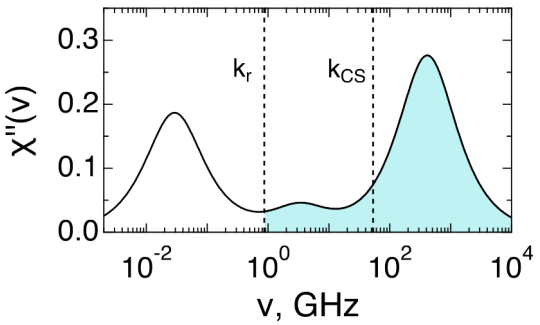

Fig. 4 Loss spectrum of the Stokes-shift dynamics for electron transfer between the bacteriopheophytin and primary quinone cofactors of the photosynthetic bacterial reaction center.[19] The shaded area shows the part of the Stokes-shift spectrum contributing to the nonergodic reorganization energy. The vertical dashed lines indicate the values of experimental rate constant ($k_r/(2\pi)$) and the rate constant for primary charge separation ($k_{CS}/(2\pi)$) in the reaction center. Adapted with permission from Ref. [19]. Copyright 2013 of the Royal Society of Chemistry.

The full Fourier transform of the time correlation function $\bar{C}_X(\omega)$ follows from $\tilde{C}_X(\omega)$ as $\bar{C}_X(\omega) = 2\text{Re}\left[\tilde{C}_X(\omega)\right]$. The frequency-domain FDT establishes the relation between the loss function (power spectrum[44, 45]) $\chi''(\omega) = \text{Im}[\tilde{\chi}(\omega)]$ and $\bar{C}_X(\omega)$. It follows by taking the imaginary part of both sides in eqn (21)

$$\bar{C}_X(\omega) = 2k_B T\frac{\chi''(\omega)}{\omega}. \tag{23}$$

According to eqn (1), $\lambda = \beta C_X(0)/2$ is obtained by integrating $\bar{C}_X(\omega)$ over all frequencies[32]

$$\lambda = \int_0^{\infty}\frac{d\omega}{\pi\omega}\chi''(\omega). \tag{24}$$

The correlation function $C_X(t)$ is accessible from time-dependent fluorescence of photoexcited optical dyes[46] and is known as the Stokes-shift time correlation function. It is also accessible from numerical computer simulations.[47, 48] Its conversion to the loss spectrum $\chi''(\omega)$ provides a convenient graphical representation of the relaxation spectrum of the medium affecting charge transfer.[19] For multi-exponential decay of the correlation function $C_X(t)$, the loss spectrum becomes a sequence of Debye peaks, with the peak position pointing to the inverse relaxation time and its amplitude to the relative contribution of a specific relaxation process to the overall reorganization energy given as the overall area under the $\chi''(\omega)/(\pi\omega)$ curve (Fig. 4). Restricting the range of integration leads to the nonergodic reorganization energy discussed below.

4 Physical models of reorganization energy

The results presented so far are very generic. They combine Gaussian statistics of the energy gap with dynamics through the Stokes-shift time correlation function. This general framework can be amended with specific physical mechanisms when microscopic interactions of the transferring electron with the surrounding medium are introduced. Before proceeding to this next step,

View Article Online
DOI: 10.1039/D2CP06072H

we briefly discuss the model of linear coupling between the quantum subsystem and harmonic thermal bath. This model, which has strongly influenced theory development, forms the basis of theories of radiationless transitions in condensed materials,[49] including Marcus theory.

4.1 Linear coupling to a harmonic bath

The power spectrum $\chi''(\omega)$ which integrates to the reorganization energy according to eqn (24) can be mapped on a bath of harmonic oscillators with distributed resonance frequencies to which the transferring electron is coupled through a function linearly depending on oscillator displacements.[45, 50] To simplify the discussion, we consider only one oscillator with the effective force constant κ representing the harmonic medium. The electron-medium interaction is a linear function of the oscillator displacement q with the coupling constant C_i depending on the electron-transfer state. Two instantaneous energies $E_i(q)$ establish the fluctuating energy gap $\Delta E(q) = E_2(q) - E_1(q)$

$$E_i(q) = E_{0i} - C_i q + \tfrac{1}{2}\kappa q^2. \tag{25}$$

Here, E_{0i} are the gas-phase energies unaffected by the medium.

The electron-medium coupling constant C_i carries the physical meaning of a Hookean external force stretching the harmonic oscillator to the equilibrium distance

$$q_{0i} = \kappa^{-1} C_i. \tag{26}$$

Given that displacements are different in two electronic states, the linear coupling model turns into the picture of two shifted parabolas along the coordinate q. The energy gap becomes a linear function of q and the functions $E_i(q)$ from eqn (25) can be projected on two Marcus parabolas through eqn (9). These two parabolas, now plotted against the reaction coordinate X, have the curvature

$$\lambda = \tfrac{1}{2}\kappa^{-1}\Delta C^2, \tag{27}$$

where $\Delta C = C_2 - C_1$. The Stokes-shift reorganization energy becomes

$$\lambda^{\mathrm{St}} = \tfrac{1}{2}\Delta C\,[q_{02} - q_{01}] = \lambda. \tag{28}$$

The linear coupling model projects Gaussian fluctuations of the medium onto Gaussian fluctuations of the energy gap. The reaction free energy becomes $\Delta F_0 = \Delta E_0 - C_2^2/(2\kappa) + C_1^2/(2\kappa)$ with $\Delta E_0 = E_{02} - E_{01}$.

4.2 Microscopic models of medium reorganization

The linear model is a phenomenological description of physical nonlinear microscopic interactions between the transferring electron and the surrounding medium. The electronic quantum-mechanical eigenvalues for the donor and acceptor states are modulated by interactions with the medium leading to electron transfer, a radiationless transition requiring resonance. In most cases, the interaction with the medium is weak compared to intramolecular excitation energies $\Delta E_{0,mn} = E_{0m} - E_{0n}$ between eigenstates of the unperturbed donor-acceptor complex. One can therefore apply the quantum-mechanical perturbation theory in terms of the electron-medium interaction Hamiltonian H'

$$E_i = E_{0i} + \langle\psi_i|H'|\psi_i\rangle + \sum_{j\neq i}\frac{\langle\psi_i|H'|\psi_j\rangle\langle\psi_j|H'|\psi_i\rangle}{\Delta E_{0,ij}}. \tag{29}$$

The first term describes the direct interaction of the transferring electron with the medium and the second refers to polarization of the electronic density and accounts for polarizability corrections. If the first terms is expanded into a series in respect to the medium coordinate q, the linear term becomes $-C_i q$ in eqn (25).

One can alternatively assign a microscopic interaction potential, of electrostatic origin, between the transferring electron and a given molecule in the liquid to write the first term in eqn (29) as a sum of all individual interactions $v_i(j)$ with N molecules in the liquid

$$E_i = E_{0i} + \sum_j v_i(j). \tag{30}$$

Since molecules of a polar medium carry molecular multipoles, of which the dipole moment is most significant for polar molecular liquids, the index j specifies both the position and orientation of a given molecule in the medium.[51] Given that the distribution of molecular charge in the donor-acceptor complex changes upon electron transfer, the interaction potential $v_i(j)$ is different in two electron-transfer states and the difference $\Delta v(j) = v_2(j) - v_1(j)$ is responsible for fluctuations of the energy gap.

From eqn (30), one can immediately proceed to calculate the energy-gap variance in eqn (1) to obtain[51, 52]

$$\lambda = \tfrac{1}{2}\beta\rho\int d1d2\Delta v(1)\Delta v(2)\,[\delta(1,2) + \rho h(1,2)]. \tag{31}$$

Here, $\delta(1,2)$ denotes the delta-function in both coordinates and orientations and $h(1,2)$ is the statistical binary correlation function of the particles in the medium; $\rho = N/V$ is the number density of N liquid molecules occupying the volume V. The pair distribution function of the medium[51] $g(1,2)$ is connected to the correlation function through the equation $g(1,2) = 1 + h(1,2)$.

In the case of electron transfer in polar liquids, one can be more specific and define the interaction of the electric field difference $\Delta\mathbf{E}_0$ of the transferring electron with the dipole moment $\mathbf{m}_j$ of molecule j in the liquid

$$\Delta v(j) = -\mathbf{m}_j \cdot \Delta\mathbf{E}_0. \tag{32}$$

The liquid fluctuations are composed in this case of dipole translations and rotations. In terms of the correlation function $h(1,2) = h^0(r_{12}) + h^{\mathrm{or}}(r_{12}, \omega_1, \omega_2)$, translations and rotations are mathematically reflected by a sum of the isotropic component $h^0(r_{12})$, depending only on the intramolecular separation r_{12}, and the orientational component $h^{\mathrm{or}}(r_{12}, \omega_1, \omega_2)$ depending on both the separation and orientations of two molecules in the liquid specified by Euler angles $\omega_{1,2}$. Substituting this correlation function to eqn (31), one arrives at the reorganization energy as a sum of the component produced by orientational fluctuations of dipoles in the liquid, λ_p, and the density component, λ_d

$$\lambda = \lambda_p + \lambda_d. \tag{33}$$

The convolution of two 3D space integrals in eqn (31) is sim-

View Article Online
DOI: 10.1039/D2CP06072H

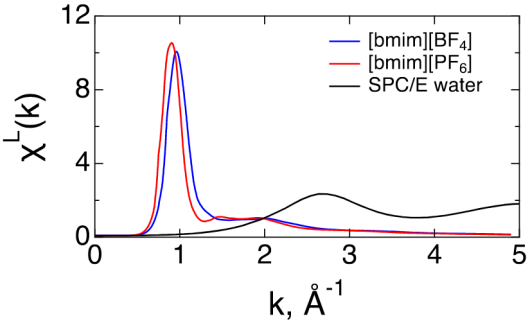

Fig. 5 Longitudinal susceptibilities $\chi^L(k)$ of [bmim][PF_6] and [bmim][BF_4] ILs calculated from MD simulations at $T = 300$ K.[53] They are compared to $\chi^L(k)$ for SPC/E water[54] at the same temperature. Adapted with permission from Ref. [53]. Copyright 2020 American Chemical Society.

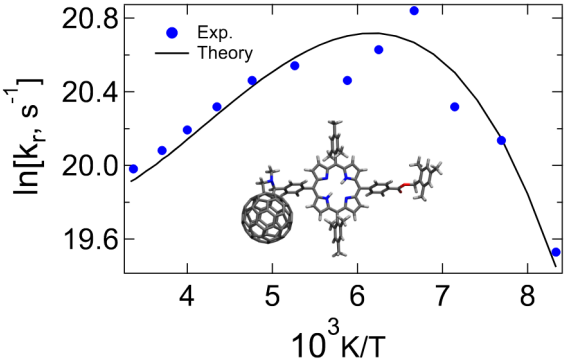

Fig. 6 Arrhenius plot for the rate constant of charge recombination in for the porphyrin-fullerene donor-acceptor dyad (inset) in 2-methyltetrahydrofuran used as a solvent. The points represent experimental data and the solid line refers to theoretical calculations.[62] Adapted with permission from Ref. [62]. Copyright 2016 American Chemical Society.

plified in reciprocal space. The orientational component can be expressed in terms of the longitudinal k-dependent susceptibility function[55, 56] $\chi^L(k)$

$$\lambda_p = \frac{1}{2}\int \frac{d\mathbf{k}}{(2\pi)^3}\left|\Delta\tilde{\mathbf{E}}_0(\mathbf{k})\right|^2 \chi^L(k). \tag{34}$$

Following original dielectric formulations of the theory,[1] the susceptibility function is often related to the k-dependent dielectric constant of the liquid[57, 58] $4\pi\chi^L(k) = \varepsilon_\infty^{-1} - \varepsilon_L(k)^{-1}$, which can be viewed as the k-dependent Pekar factor.[59] In this relation, ε_∞ is the high-frequency dielectric constant and the longitudinal dielectric function $\varepsilon_L(k)$ becomes the static dielectric constant ε_s in the continuum limit $k \to 0$, when one arrives at the standard Pekar factor

$$c_0 = \varepsilon_\infty^{-1} - \varepsilon_s^{-1}. \tag{35}$$

This polarity parameter enters all traditional continuum theories of polarons[59, 60] and electron transfer[1] in polar materials.

An important property of $\chi^L(k)$ is that it reaches a plateau at small wavevectors k at the level $\chi^L(k) \simeq \chi^L(0) = (4\pi)^{-1}c_0$ (solid black line in Fig. 5). At a sufficiently large size of the donor-acceptor complex, $\chi^L(k)$ can be replaced with $\chi^L(0)$ in the k-integral in eqn (34). The result is the dielectric formulation for the medium reorganization energy. If the donor and acceptor are viewed as two spheres with, correspondingly, radii R_D and R_A separated by the distance R, one arrives at the Marcus equation for the medium reorganization energy

$$\lambda = c_0 e^2\left(\frac{1}{2R_D} + \frac{1}{2R_A} - \frac{1}{R}\right). \tag{36}$$

Importantly, $\lambda \propto \beta$ present in eqn (1) disappears from the final equation because of the macroscopic, $k \to 0$ limit adopted for the susceptibility. The disappearance of the β factor is a consequence of the long-range character of dipolar interactions allowing one to arrive at the limit of macroscopic Johnson-Nyquist noise. The reorganization energy λ_p still depends on temperature through the liquid expansivity for experiments performed at constant pressure, but the overall temperature dependence is weak.

The above arguments do not apply to the density component λ_d in eqn (33). Because of the short range of the density fluctuations largely driven by an entropic penalty to re-arrange the molecular repulsive cores, the scaling

$$\lambda_d \propto T^{-1} \tag{37}$$

is maintained and the overall explicit dependence on temperature becomes $\lambda = a + b/T$. The density component of the reorganization energy is the main contributor to its decaying temperature dependance[61] resulting in an observable bell-shaped form of the Arrhenius plot.[62] Figure 6 shows experimental results for the charge-recombination rate constant in a porphyrin-fullerene donor-acceptor dyad[63] measured in a wide range of temperatures available for 2-methyltetrahydrofuran used as a solvent. The solid line in the plot comes from theoretical calculations allowing good account of the measurements. The assumption of a temperature-independent λ leads to the canonical straight line of the Arrhenius law and cannot be reconciled with the data.

When the temperature dependence of the reorganization energy is not concerned, continuum dielectric theories (e.g., eqn (36)) provide reasonable estimates of the magnitude of λ. This is not the case anymore for electron transfer in ionic liquids (ILs). ILs are conducting liquids composed of opposite sign ions. Strong Coulomb interactions in ionic pairs produce quasiperiodic ordering of opposite-charge ions[64, 65] reflected by a sharp peak of $\chi^L(k)$ found by molecular dynamics (MD) simulations[53, 66] (Fig. 5). This sharp peak contributes significantly to the reciprocal-space integral in eqn (34), invalidating the dielectric continuum limit when applied to solvation in ILs. The limit $k \to 0$ taken in $\chi^L(k)$ to arrive to eqn (36) does not apply to ILs and the phenomenology of continuum solvation does not extend to ILs as media for electron transfer. The peak of $\chi^L(k)$ in molecular polar liquids is lower in magnitude and is positioned at higher k-values, as illustrated with calculations done for SPC/E water[67] in Fig. 5. A more collective structural ordering in ILs shifts the peak to lower k-values making it essential for the reciprocal-space calcu-

View Article Online
DOI: 10.1039/D2CP06072H

lations.

4.3 Medium polarizability

The appearance of the high-frequency dielectric constant ε_∞ in the Pekar factor (eqn (35)) is a reflection of the separation of time scales when electronic polarization follows adiabatically all slower degrees of freedom.[1, 68] A full account of molecular electronic polarizability requires microscopic liquid-state theories,[69] but a substantial simplification is achieved by adopting Frohlich's model[70] in which permanent molecular dipoles are immersed in a continuum dielectric with the dielectric constant ε_∞. Electrostatic interactions between the transferring electron and the medium dipoles become screened by the electronic polarization such that the dipole moment m in eqn (32) is multiplied with the screening parameter q to become[71] qm. The value of q consistent with simulations[68] is the Lorentz cavity factor[72]

$$q = \frac{\varepsilon_\infty + 2}{3\varepsilon_\infty}. \tag{38}$$

This formulation replaces the microscopic susceptibility function $\chi^L(k)$ in eqn (34) with a screened function to produce a new medium polarity parameter in its continuum, $k \to 0$, limit

$$4\pi\chi^L(0) = q^2\left(1 - \varepsilon_s^{-1}\right). \tag{39}$$

This polarity parameter, which should replace c_0 in the standard Marcus eqn (36), turns out to be close numerically to the original Pekar factor. Figure 7a shows $4\pi\chi^L(0)$ from eqn (39) vs c_0 for 15 common molecular solvents (see the full list in the Supplementary Material (SM)). For most practical purposes, either of the two can be used in continuum models for the reorganization energy.

From the microscopic perspective, addition of electronic polarizability to a fluid of molecules carrying permanent dipole moments produces two effects: (i) screening of electrostatic interactions and (ii) an increase of the effective, mean-field molecular dipole from the gas-phase value m to an effective condensed-matter dipole[69] m'. These two effects oppose and mostly compensate each other in the reorganization energy: λ is found to be nearly unchanged when ε_∞ is increased while keeping m constant.[68] Polarizability corrections in numerical simulations is a separate issue.

Nonpolarizable force fields of molecular liquids assign an adjusted, condensed-matter dipole m' to molecules. For instance, the dipole moment of SPC/E water, $m' = 2.35$ D, is substantially higher than its gas-phase value $m = 1.89$ D. Simulations with nonpolarizable force fields do not include screening by electronic polarization and corrections are required.[73–75]

A universal correction scheme is not possible since the ratio of λ values in a polarizable solvent and in its nonpolarizable mimic, incorporating polarizability in terms of the effective dipole m', depends on solvent polarity.[74] Figure 7b presents λ calculated from eqn (34) with a full account for the polarizability effects and for a corresponding mimic solvent with $\varepsilon_\infty = 1$ and the molecular dipole m' (see SM). The dimensionless reorganization energies $\lambda\sigma_s/e^2$ (σ_s is the molecular diameter) scale approximately linearly with the dimensionless density of dipoles (in Gaussian units)

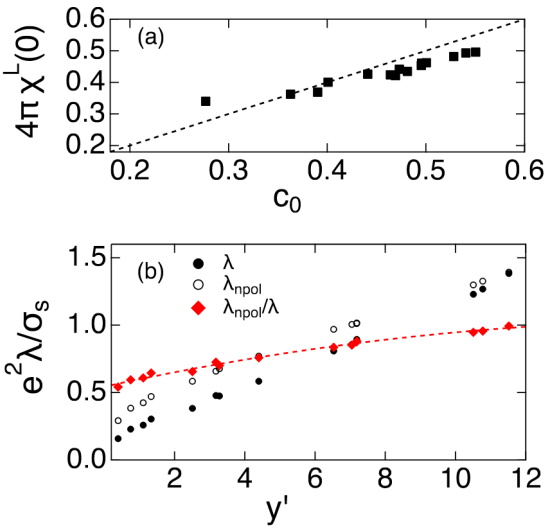

Fig. 7 (a) The polarity parameter in eqn (39) vs the Pekar parameter c_0 (eqn (35)) for 15 polar molecular solvents (see SM for details). The dashed line specifies the equality line to guide the eye. (b) Reorganization energy of the two-sphere configuration with $R_D = R_A$ (eqn (36)) vs the solvent dipolar density y' (eqn (40)); $R_D/\sigma_s = 1$. Calculations are done with the full account of the polarizability effects (λ, filled points) and for nonpolarizable solvents with $\varepsilon_\infty = 1$ and the effective dipole m' assigned to the liquid molecules (λ_{npol}, open points). Red points indicate the ratio λ_{npol}/λ and the dashed line is a polynomial fit through the points: $0.544 + 0.057y' - 0.00163(y')^2$.

$$y' = \frac{4\pi}{9}\beta\rho(m')^2. \tag{40}$$

[This parameter becomes $\beta\rho(m')^2/(9\varepsilon_0)$ in SI units, where ε_0 is the vacuum permittivity]. The ratio of λ_{npol}/λ is close to unity for highly polar solvents, but drops to $\simeq 0.6$ at lower polarities. For water, one obtains a correction factor $\simeq 0.8$. It should be used to multiply λ in nonpolarizable force-field solvents to account for the screening effects.

5 Nonergodicity and nonparabolicity

The construction[1] and experimental verification[38] of Marcus theory is a monumental development in science based on fundamental ideas of Gaussian statistics, Gibbsian ensembles, and fluctuation-dissipation relations connecting the spread of fluctuating localized quantum states to thermal energy of the medium. It provides a sufficiently simple two-parameter description of the reaction activation barrier requiring the reorganization energy and the reaction free energy as input parameters (eqn (19)). The medium reorganization energy finds its firm foundation in electrostatics of interactions of the donor and acceptor molecules with the polarizable medium. This microscopic foundation is the physical motivation for applying the central limit theorem and Gaussian statistics of X and the reason for a relatively narrow range of λ values in polar media.

The monumental character of the theory is also a source of its rigidity toward parameter manipulations to achieve faster charge

View Article Online
DOI: 10.1039/D2CP06072H

separation critical to the operation of both artificial and natural photosynthesis. Nature relies on vectorial, trans-membrane electron transport through chains of cofactors in its energy chains for all energy needs.[25] One wonders if Marcus theory provides a sufficiently solid foundation for describing hopping electron transport in biology and can be equally applied to developing strategies for man-made devices to transform solar energy to separation of charges.

Two major difficulties arise when applying Marcus theory to biological hopping electron transport, and they both are implicit to the inverted Marcus parabola, that is $-\beta\Delta F^{\dagger}$ vs $-\Delta F_0$, specified by eqn (19). First, a large negative reaction free energy (positive driving force $-\Delta F_0$) is required to eliminate the activation barrier and bring the donor and acceptor energy levels to tunneling resonance. Such large driving forces are usually not found in biological electron-transport chains, which often operate at near-zero driving force. The reorganization energy often exceeds $\simeq 1$ eV for reactions in solution and is believed to be somewhat smaller, $\simeq 0.8$ eV, for protein electron transfer.[76] Such large activation barriers often produce electron-transfer rates too slow for an efficient charge transport.[77] Independently of specific measurements and theories and numerical algorithms to interpret experimental data, a fundamental question persistent in the electron-transfer field is whether new physical mechanisms can be identified that potentially eliminate energy bottlenecks predicted by Marcus theory and allow lower reorganization energies and maximum rates at lower driving forces.

What is described next is an attempt to step beyond the limits of the Marcusian straitjacket and to identify scenarios for lowering the reorganization energy and altering the energy-gap law. As is nearly universally the case, nature has already identified such mechanisms and one needs to turn to protein electron transfer and natural photosynthesis for clues and inspiration.

5.1 Nonlinear (non-parabolic) effects

The linear coupling model specified by eqn (25) requires that the Hookean force constant κ stays the same in both electron-transfer states. This requirement physically implies that the structure of the medium is not altered by the transferring electron. This is not true for most problems involving small ions since the liquid structure is strongly affected by the ionic charge. However, many donor and acceptor molecules are large, thus reducing the strength of electrostatic interactions with the solvent. In addition, the long range of the Coulomb interaction involves many molecules not in immediate contact with the donor or acceptor and the structural variations get averaged out.

There are several physical situations when altering the force constant of medium fluctuations is required. The most straightforward case is the alteration of the frequencies of donor and acceptor vibrations related to changing oxidation state[78, 79] (also through Duschinsky rotations of normal modes[80]). The second set of problems is brought by the second-order perturbation term in eqn (29). If the donor-acceptor complex is polarizable, this term produces the free energy of electronic polarization $-\frac{1}{2}\mathbf{E}_s\cdot\boldsymbol{\alpha}_i\cdot\mathbf{E}_s$ by the medium electric field $\mathbf{E}_s$. This term is quadratic in the solvent electric field viewed as a collective solvent coordinate. If the polarizability of the donor-acceptor complex $\boldsymbol{\alpha}_i$ changes between two states, the effective Hookean force constant of the medium fluctuations gains a dependence on the electron-transfer state. In all these cases, and potentially in many others, the linear coupling model (L-model, eqn (25)) needs to be generalized to the quadratic coupling model (Q-model) with the energy states defined by the following equation

$$E_i(q) = E_{0i} - C_i q + \tfrac{1}{2}\kappa_i q^2. \tag{41}$$

The reason for the name is that the energy gap is now a linear-quadratic function of the medium coordinate: $\Delta E(q) = -\Delta C q + \frac{1}{2}\Delta\kappa q^2$, $\Delta\kappa = \kappa_2 - \kappa_1$.

Independently of physical reasons for altering the force constant, the Q-model provides a first glimpse into the world beyond the Marcus framework. Like the latter (L-model), the Q-model allows an exact mathematical solution for the free energy surfaces within Gibbsian statistics for assigning statistical weights to different system configurations. The result is[81]

$$\begin{aligned} F_1(X) &= \left(\sqrt{|\alpha||X - X_0|} - \sqrt{\alpha^2\lambda_1}\right)^2, \\ F_2(X) &= \Delta F_0 + \left(\sqrt{|1+\alpha||X - X_0|} - \sqrt{(1+\alpha)^2\lambda_2}\right)^2. \end{aligned} \tag{42}$$

The parameter X_0 here is related to the reaction free energy ΔF_0 through the following equation

$$X_0 = \Delta F_0 - \lambda_1\frac{\alpha^2}{1+\alpha}. \tag{43}$$

The free energy surfaces are nonparabolic and the model allows separation of the Stokes-shift and variance reorganization energies according to the rule

$$\lambda_2 < \lambda^{\mathrm{St}} < \lambda_1. \tag{44}$$

The 1,2 indexes here can be swapped: the main result is that λ^{St} falls between two unequal variance reorganization energies. The extent of non-parabolicity is controlled by the non-parabolicity parameter

$$\alpha = \frac{2\lambda^{\mathrm{St}} + \lambda_2}{\lambda_1 - \lambda_2}. \tag{45}$$

It tends to infinity in the Marcus limit $\lambda_1 = \lambda_2$ when the free energy surfaces become crossing Marcus parabolas.

As mentioned above, even though structural solvent changes around charged donor and acceptor are possible and lead to established non-parabolicity effects for small ions,[83] simulations often find Marcus parabolas well justified for larger donor and acceptor molecules in polar solvents.[84, 85] The situation can change for protein electron transfer. Proteins are highly packed media with little room in their cores for structural changes. However, water is a light and mobile part of the thermal bath that can respond to altering charge distribution by wetting parts of the protein core (electrowetting). There is increasing evidence, mostly from computer simulations,[86–89] that water can pen-

View Article Online
DOI: 10.1039/D2CP06072H

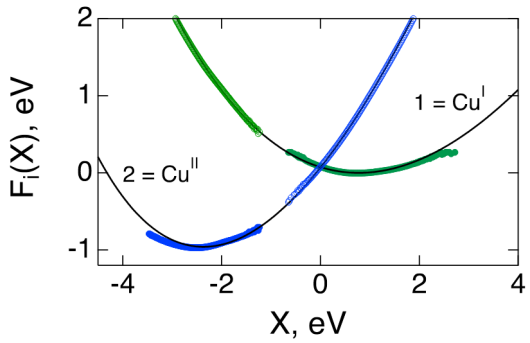

Fig. 8 Free energy surfaces for electron transfer between the $Cu^{I/II}$ active site and the nearby tryptophan residue of azurin calculated in the Q-model (solid lines) and obtained from MD simulations (points).[82] The upper portions of the simulation data are obtained from the results around the minima by applying the linear relation from eqn (10). The reorganization energies are: $\lambda_1 = 2.09$ eV, $\lambda_2 = 1.17$ eV, and $\lambda^{St} = 1.65$ eV (see eqn (44)). Adapted with permission from Ref. [82]. Copyright 2022 American Chemical Society.

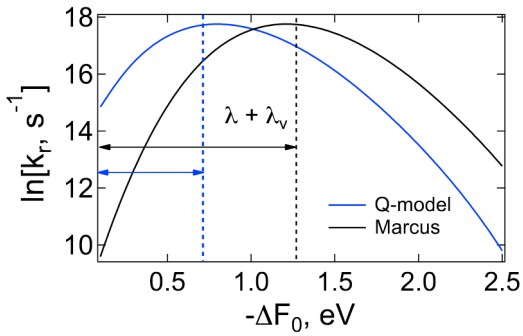

Fig. 9 Energy gap law for the Marcus model (black line) and for the Q-model (blue line). The position of the top of the inverted parabola shifts from $\lambda + \lambda_v$ in Marcus model to $\lambda_v + \lambda\alpha/(1+\alpha)$ in Q-model. The parameters in the plot are taken from Ref. [91] where Q-model was applied to fit the experimental kinetic data.[38]

etrate into active sites of redox-active proteins in response to changing oxidation state or light activation.[90] When this happens, the protein-water thermal bath changes its structure between two oxidation states and the force constant becomes state-dependent as described by Q-model (eqn (41)). The resulting free-energy surfaces are non-parabolic as is shown in Fig. 8 for electron transfer between the $Cu^{I/II}$ active site and the neighboring tryptophan residue in the azurin protein. Simulations provide the portions of the free energy surfaces close to their minima and the upper parts of each curve are obtained from the linear free-energy relation (eqn (10)).[82] The Q-model provides the picture of crossing non-parabolic free-energy surfaces with different curvatures at their corresponding minima.

The Q-model offers advantages for the energy efficiency of charge transfer by lowering the driving force required to achieve activationless reactions. The activation barrier vanishes for forward electron transfer at $X_1 = 0$ (eqn (19)), which in Q-model becomes

$$X_1 = \Delta F_0 + \lambda_1 \frac{\alpha}{1+\alpha}. \tag{46}$$

The driving force $-\Delta F_0 = \lambda$ required to reach the top of the Marcus inverted parabola becomes $-\Delta F_0 = \lambda\alpha/(1+\alpha)$ within the Q-model. For instance $-\Delta F_0 = \lambda/2$ at $\alpha = 1$. When intramolecular reorganization energy λ_v is taken into account (see below), the top of the inverted parabola becomes $\lambda_v + \lambda$ in Marcus model, but is $\lambda_v + \lambda\alpha/(1+\alpha)$ in Q-model. The overall shift of the maximum of the inverted parabola to lower values of the driving force is illustrated[91] in Fig. 9 for the donor-acceptor charge-transfer complex studied by Miller and coworkers.[38]

5.2 Fast transitions in slow media

Equation (24) defines the reorganization energy as the entire energy dissipated to the medium in the form of heat when electron is transferred and allowed to relax. Energy dissipation at a given frequency,[43] $\propto \omega\chi''(\omega)$, is given by the loss spectrum $\chi''(\omega)$ (Fig. 4). The variance reorganization energy λ thus reflects the fluctuation-dissipation philosophy stipulating that the medium modes that dissipate the most are those that fluctuate the most. The relative significance of different relaxation processes contributing to the overall thermodynamic λ is specified by amplitudes of the corresponding relaxation peaks in $\chi''(\omega)$.

The interpretation of λ as the frequency integral over the loss spectrum calls for its extension to processes when the thermodynamic view becomes limited. When some essential relaxation modes of the medium become slower than the reaction time $\tau_r = k_r^{-1}$, they do not contribute anymore to reaction's activation on the observation time τ_r. This limitation sets up a constraint on the phase space available for sampling, which makes the distribution of system's statistical configurations non-Gibbsian.[92, 93] This new statistics defines the nonergodic reorganization energy becoming essential when the rate constant k_r imposes a low-frequency cutoff on the loss spectrum[94] (Fig. 4)

$$\lambda(k_r) = \int_{k_r}^{\infty} \frac{d\omega}{\pi\omega} \tilde{\chi}''(\omega). \tag{47}$$

The nonergodic reorganization energy $\lambda(k_r)$ depends on the reaction rate k_r and turns into the standard, thermodynamic reorganization energy at $k_r \to 0$. It is obvious that $k_r \to 0$ is a mathematical idealization and, realistically, the thermodynamic limit is achieved when the reaction time τ_r becomes longer than the relaxation time τ_{slow} of the slowest medium mode noticeably contributing to λ.

Primary charge separation in bacterial reaction centers is an important application of this concept. The reorganization energy,[17] $\lambda(k_r) \simeq 0.35$ eV, arises from restricting the fluctuation spectrum of the protein-water thermal bath on the reaction time scale $\tau_r \simeq 3 - 10$ ps. This value is a significant reduction from the equilibrium reorganization energy $\lambda \simeq 2.46$ eV achieved by computer simulations with the simulation time of 10 ns.[23]

The phenomenology of frequency cutoff introduced by the reaction rate should generally apply to fast reactions in media with dispersed relaxation times allowing both fast and slowly relaxing processes coupled to electron transfer. From the experimental

View Article Online
DOI: 10.1039/D2CP06072H

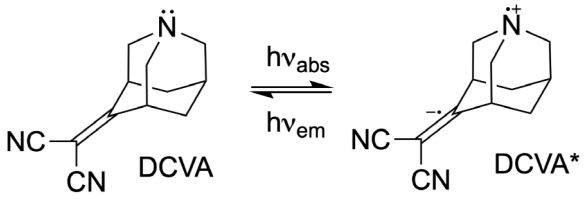

Fig. 10 Charge transfer in DCVA molecule.[99]

side, alteration of the spectroscopic Stokes shift through the solvent glass transition[95] is accurately described[96] by eqn (47). Another recent example[97] concerns the reorganization energy in ionic liquids. Spectroscopic studies of charge-transfer bands in the DCVA chromophore[98, 99] (Fig. 10) dissolved in ionic liquids produced a surprising result of the reorganization energy close in magnitude to that measured in cyclohexane (see below). On the other hand, the equilibrium reorganization energies calculated from eqn (34) with the structure factors shown in Fig. 5 are significantly higher (horizontal lines in Fig. 11). The resolution of the puzzle is found in terms of eqn (47): the short lifetime of the photoexcited chromophore $\tau_e \simeq 200$ ps imposes a frequency cutoff $k_r = \tau_e^{-1}$ on the loss spectrum producing the nonergodic reorganization energy consistent with observations (Fig. 11).

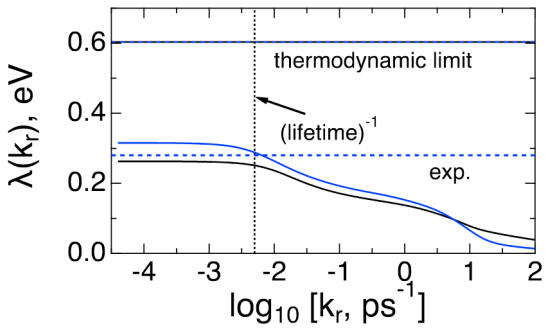

Fig. 11 Nonergodic reorganization energy $\lambda(k_r)$ (eqs (47)) for [bmim][BF_4] (IL-1) and [bmim][PF_6] (IL-2) ILs. The vertical dotted line indicates $k_r = \tau_e^{-1}$ with $\tau_e = 2 \times 10^{-10}$ s representing the lifetime of the excited state of the DCVA chromophore[99] shown in Fig. 10. The horizontal lines, indistinguishable on the plot scale, indicate the equilibrium values of the reorganization energy for IL-1 and IL-2 calculated from eqn (34) with the susceptibility functions shown in Fig. 5. The dashed horizontal line marked "exp." indicates the reorganization energy from the band-shape analysis of DCVA. Adapted with permission from Ref. [97]. Copyright 2022 American Chemical Society.

5.3 Nonergodic sampling

Both the standard Marcus formulation[6] and the Q-model[81] employ Gibbsian statistics for statistical averages. It is based on the assumption of ergodicity implying that all essential configurations have been sampled on the time of observation. This does not have to be always the case. Some parts of the configuration space could be unreachable to the system, either by geometrical constraints, such as those imposed by the protein fold, or through dynamical restrictions requiring times too long to reach those configurations. A well-known example is the second-order phase transition of spontaneous magnetization, when half of the phase space specifying the macroscopic magnetic dipole either "up" or "down" is dynamically restricted by the diverging time required to flip it.

Glassy dynamics and glass transition provide examples of non-Gibbsian sampling more relevant to the statistics of proteins.[100] The phase space of such media is broken[92] into "components" such that the transition time between components exceeds the observation time. The separation of the system phase space into components breaks the system symmetry since the symmetry of the distribution function, due to imposed constraints, is lowered compared to the symmetry of the Hamiltonian.[93] The result is that the statistical weights assigned to system configurations do not strictly follow the Gibbsian recipe.

The change in statistical sampling propagates to the breakdown of the link between the first and second moments of the reaction coordinate X stipulated by the static limit of the fluctuation-dissipation theorem.[101, 102] For the stretched Hookean oscillator considered in eqn (25), the connection between the first and second statistical moments is established through the linear susceptibility connecting the stationary displacement reached at $t \to \infty$ to the force applied at $t = 0$

$$\Delta q = \chi C. \tag{48}$$

For an unconstrained oscillator stretched by force C, the susceptibility $\chi = \kappa^{-1}$ is the inverse force constant. It provides access to both the variance and Stokes-shift reorganization energies in eqn (27) and (28).

Constraints imposed on the configurations available to the system can have different physical origin, but they lead to common phenomenology when applied to electron transfer. Instead of the equality between the Stokes-shift and variance reorganization energies in the Gibbsian formulation (eqn (17)), one finds the following inequality[32]

$$\lambda^{\mathrm{St}} < \lambda. \tag{49}$$

The free energy surfaces are still parabolas for the linear coupling model, but with curvatures not related to the separation between their minima specified by $2\lambda^{\mathrm{St}}$ (Fig. 3). The effective reaction reorganization energy, that is the reversible work required to move along the first surface to the position of the second minimum, is reduced, because of the lower curvature, to the following "reaction" reorganization energy

$$\lambda^r = \frac{(\lambda^{\mathrm{St}})^2}{\lambda} < \lambda^{\mathrm{St}}. \tag{50}$$

Crossing of the free energy surfaces still defines the activation barrier and the standard Marcus formula can be reformulated from eqn (19) to a form in which λ^r replaces λ

$$\Delta F^{\dagger} = \frac{(\Delta F_0' \pm \lambda^r)^2}{4\lambda^r}. \tag{51}$$

Importantly, the reaction free energy $\Delta F_0'$ in Eq. (51) is distinct from the equilibrium free energy entering Marcus equation (Eq.

View Article Online
DOI: 10.1039/D2CP06072H

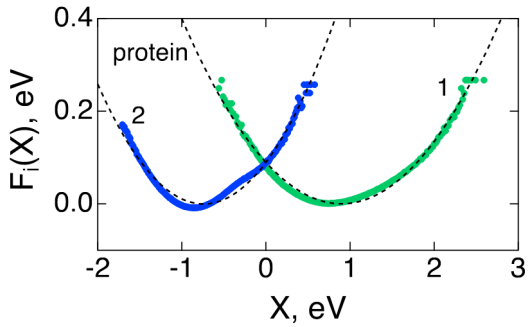

Fig. 12 Free energy surfaces for electron transfer between the $Cu^{I/II}$ active site of azurin and the nearby tryptophan residue. Shown is the calculation from MD simulations (points) based on the protein component of the thermal bath. The dashed lines are fits to parabolas with unequal curvatures. The free energy surfaces labeled as in Fig. 8 are plotted with zero reaction free energy. The ratio λ^{St}/λ is 0.34 for $1 \to 2$ transition and 0.64 for $2 \to 1$ transition. Adapted with permission from Ref. [82]. Copyright 2022 American Chemical Society.

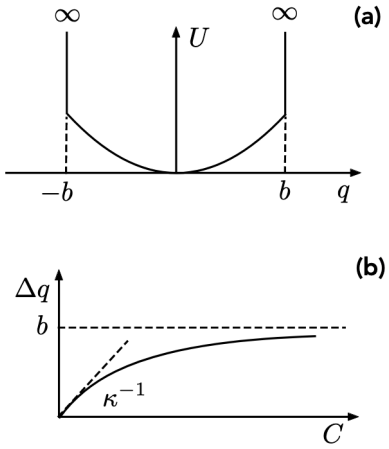

Fig. 13 (a) Potential energy $U(q)$ of the constrained harmonic oscillator $-b < q < b$. (b) Displacement Δq of the constrained oscillator in response to the external force C. The susceptibility deviates downwards from the linear response $\chi = \kappa^{-1}$ as the pulling force increases and the equilibrium position of the stretched oscillator approaches the constraining boundary.

(19)). It is reduced by the same nonergodicity factor as the reaction reorganization energy in Eq. (50)

$$\Delta F_0' = \Delta F_0(\lambda^{St}/\lambda). \tag{52}$$

The efficiency of the thermodynamic driving force is diminished in nonergodic media.

The nonergodic driving force applies to transitions between the donor and acceptor immersed in a nonergodic thermal bath, such as the interior of a protein. In contrast, the thermodynamic reaction free energy is often determined by measuring the equilibrium redox potentials of the cofactors removed from that specific environment and brought in contact with electrodes of an electrochemical experiment. If the activation barrier is expressed in terms of the equilibrium driving force ΔF_0, one obtains

$$\Delta F^{\dagger} = \frac{(\Delta F_0 \pm \lambda^{St})^2}{4\lambda}. \tag{53}$$

The energy gap law for $\ln k_r$ plotted against the driving force $-\Delta F_0$ still yields $-\Delta F_0 = \lambda^{St}$ at the top of the inverted parabola. This plot thus gives information about λ^{St}, while the parabola's curvature provides λ.

A number of simulations of protein electron transfer[103, 104] have produced $\lambda^{St} \simeq 0.7 - 0.8$ eV consistent with observations.[24, 105] However, a significantly larger value of λ lowers the reaction reorganization energy λ^r entering the activation barrier. Equations (51) and (53) thus predict different reorganization energies when evaluated from the energy gap law and from the overall activation barrier obtained, for instance, from the Arrhenius slope of the reaction rate constant. This notion seems to be supported by electrochemistry of proteins. It provides direct access[106] to λ^r by scanning the electrode overpotential η, which is directly connected to $\Delta F_0'$ in eqn (51) as $e\eta = -\Delta F_0'$. Accordingly, thin-film protein electrochemistry has consistently reported $\lambda^r \simeq 0.2 - 0.6$ eV for redox-active proteins.[107–111] These values are consistently lower than $\lambda^{St} \simeq 0.7 - 0.8$ reported by solution measurements.[105]

The inequality between the reorganization energies in eqn (49) can be understood from the thermodynamic arguments. The work externally done to transfer charge should be equal (equilibrium) or higher (non-equilibrium) than the change in the system free energy.[112] The work externally done to move charge e through the potential difference $\Delta\phi$ while polarizing the environment is

$$w_{ext} = \tfrac{1}{2}e|\Delta\phi| = \lambda^{St}. \tag{54}$$

The system free energy invested in moving charge can be viewed as the free energy of solvating an effective solute interacting with the medium by the potential $\Delta V = \sum_j \Delta v(j)$ (eqn (32)). By applying the statical perturbation theory and truncating the expansion series after the second term one gets[36] the change in the system free energy (see SM)

$$|\Delta F| = 2\lambda^{St} - \lambda. \tag{55}$$

When work is done out of equilibrium, the inequality $w_{ext} > |\Delta F|$ is required, from which eqn (49) follows.

Proteins relaxing on time scales longer than the reaction time should be viewed as nonequilibrium systems in which producing work requires energy dissipation and entropy production. Indeed, computer simulations of protein electron transfer have shown that nonergodic sampling leading to eqn (49) is mostly characteristic of large, membrane-bound protein complexes.[88, 113] For instance, the variance reorganization energy was found to increase continuously, without saturation in MD simulations of the membrane-bound bc_1 complex[32] when longer observation windows from the simulation trajectory (~ 15 μs) were allowed. Similarly, attempts to converge relaxation times for the distance dynamics between protein residues have lead to relaxation times growing linearly with sampling time.[114]

The protein medium is the main component of the thermal bath producing nonergodic statistics of configurations. Hydration wa-

View Article Online
DOI: 10.1039/D2CP06072H

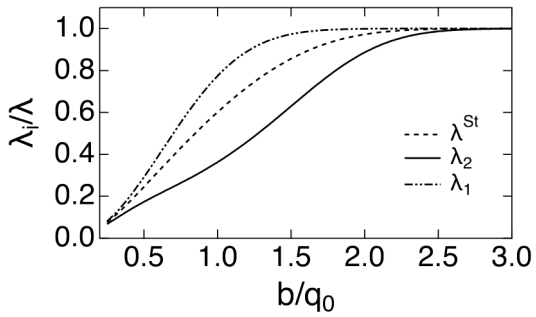

Fig. 14 Reorganization energies λ_1 ($C = 0$), λ_2 (C), and λ^{St} vs the constraining distance b normalized with the linear equilibrium position $q_0 = C/\kappa$. The reorganization energies are normalized by the Marcus reorganization energy of the linear coupling model $\lambda = C^2/(2\kappa)$ (eqn (27)).

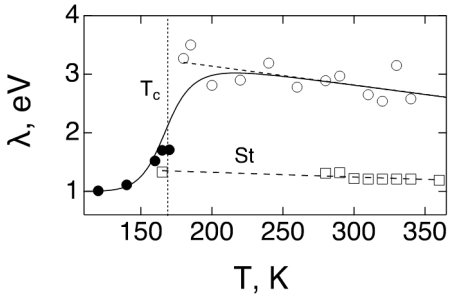

Fig. 15 Temperature dependence of the reorganization energies λ^{St} ("St", open squares) and λ (circles): $\lambda > \lambda^{St}$ at high temperatures (open circles) and $\lambda^{St} \simeq \lambda$ below the crossover temperature $T_c \simeq 170$ K (filled circles). The simulation results (points) are for the cytochrome c protein.[118] Reproduced with permission from Ref. [118]. Copyright 2018 American Chemical Society.

ter coupled to protein fluctuations substantially masks its nonergodic character for smaller globular proteins (e.g., azurin and cytochrome c). It can still be revealed by considering fluctuations produced by protein alone. They display a strong separation between λ^{St} and λ according to eq (49) (Fig. 12). The jammed and frustrated protein interior promotes glassy dynamics[100] with strong features of nonergodic sampling.[115, 116]

Nonergodic sampling of configuration space implies that the system is not allowed to reach full equilibrium and stays out of equilibrium on the reaction time scale. Following the general discussion by Reiss,[117] nonequilibrium configurations can be reached by imposing constraints on dynamic and thermodynamic variables. How to map inequality (49) on specific constraints imposed on statistics of configurations is currently not clear, but significance of constrains can be illustrated by applying a simple modification to the standard linear coupling model considered above.

In contrast to a harmonic bath displaced by the Hookean force of the electron-medium coupling considered in eqn (25), the medium oscillator is now constrained by the condition $-b < q < b$ (Fig. 13a). This constraint is equivalent to putting an infinite repulsive potential at $|q| = b$. To simplify the model, one can put $C_1 = 0$ and $C_2 = C$. It is clear from Fig. 13b that the susceptibility χ from eqn (48) should deviate downward from the linear result $\chi = \kappa^{-1}$ as C increases pulling the equilibrium displacement closer to the repulsive wall at $q = b$. The response becomes nonlinear and one anticipates the breakdown of the standard Marcus picture. While the analytical solution for the free energy surfaces $F_i(X)$ is quite complicated in this case, the Stokes-shift and variance reorganization energies are readily defined from the average position $\langle q\rangle_C$ at a given value of the electron-medium coupling C

$$\lambda^{St} = \tfrac{1}{2}C[\langle q\rangle_C - \langle q\rangle_0], \qquad \lambda_i = \tfrac{1}{2}\beta C^2\langle(\delta q)^2\rangle_i, \tag{56}$$

where two reorganization energies λ_i correspond to the variance of q calculated at C (λ_2) and $C = 0$ (λ_1).

Figure 14 shows three reorganization energies, two λ_i and λ^{St}, for the constrained medium oscillator as functions of the position of the constraining boundary b. As b increases, one arrives at the standard Marcus description when all reorganization energies converge to a single value $\lambda = C^2/(2\kappa)$ of the linear model (eqn (27)). As the repulsive boundary approaches the equilibrium position of the linear oscillator $q_0 = C/\kappa$, both the average $\langle q\rangle_C$ and the variance of q become affected, but to a different degree. One finds the reorganization energies split in a way qualitatively similar to the result of the Q-model (eqn (44)). However, this separation does not reproduce inequality (49), which is often found to apply to both variance reorganization energies,[88] $\lambda_1 \simeq \lambda_2$, in protein electron transfer. The type of constraints allowing this phenomenology is currently unknown. It is still worth noting a substantial reduction of all reorganization energies involved imposed by constrained configuration space. While inequality (49) is not satisfied by both variance reorganization energies λ_i, the main phenomenology of their strong reduction, required for functioning of natural photosynthesis and biological energy chains, is captured by the constrained oscillator model.

It appears that proteins as media for biological charge transport have to maintain nonergodic sampling of configurations to allow low activation barriers for individual charge hopping transitions. One therefore wonders if thermodynamic conditions can be altered to allow the return to the FDT commonly found for electron transfer in polar liquids. Protein dynamical transition reported by Mössbauer spectroscopy[100, 119] and by neutron scattering[120] as a crossover in the slope of atomic displacements vs temperature provides such a transition mechanism. Figure 15 illustrates this general result[118, 121] for the temperature-dependent reorganization energies of the cytochrome c redox-active protein. A significant level of nonergodicity, represented by a large extent of λ over λ^{St}, is maintained in the entire physiological range of temperatures. The protein returns to the state consistent with the FDT, $\lambda \simeq \lambda^{St}$, below the crossover temperature close to the temperature of the protein glass transition. This crossover leads to a sharp increase in the activation barrier of electron transfer and is marked by a kink in the Arrhenius plot for the reaction rate constant.

View Article Online
DOI: 10.1039/D2CP06072H

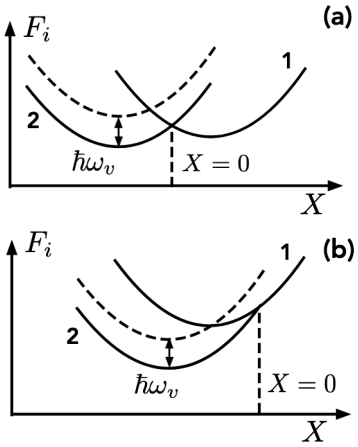

Fig. 16 Illustration of the effect of intramolecular quantum excitations on on the activation barrier in the normal (a) and inverted (b) regions of electron transfer. $X = 0$ indicates the crossing point of classical parabolas when the energy gap is used for the reaction coordinate.

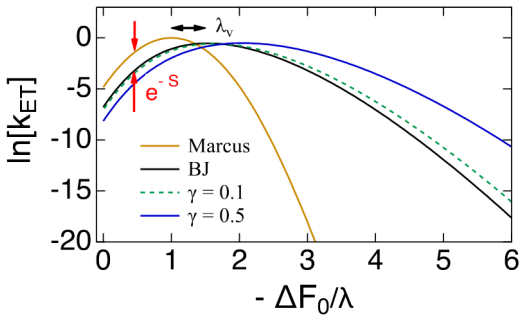

Fig. 17 Energy gap law $\ln[k_{ET}]$ vs the driving force $-\Delta F_0$ in the Marcus model (orange line) and from the Bixon-Jortner equation (BJ, black line). Two vertical red arrow marks the exponential factor $\exp[-S]$ by which the rate is lowered in the normal electron-transfer region. The horizontal arrow marks the vibrational reorganization energy λ_v by which the top of the inverted asymmetric parabola is shifted when vibrations are taken into account. Also shown are the results of eqn (59) at $\tilde{\gamma} = 0.1$ (green line) and $\tilde{\gamma} = 0.5$ (blue line); $S = 2$ and $\hbar\omega_v = 1300$ cm^{-1}.

6 Vibrational reorganization

As mentioned above, the discovery of the inverted region by Marcus was not only an amazing result of a consistent theory development, but was was also viewed as holding large significance for photo-induced charge separation (eqn (3)). As illustrated in Fig. 1, this is ensured by putting forward charge separation in the near-activationless region and backward charge recombination in the inverted region of electron transfer.

The picture of crossing parabolas was established for classical medium modes and requires modification if some of vibrational energies exceed the thermal energy: $\hbar\omega_v > k_B T$ (quantum regime). The problem was solved for radiationless transitions in solids,[4, 26, 78, 122] before Marcus took on electron-transfer reactions in polar liquids.[1] Bixon and Jortner later adopted[27, 123] the Huang and Rhys solution[26] to derive a convenient expression for the rate constant in the limit of a quantum mode q coupled linearly to the transferring electron, which thus becomes the quantum limit of the linear model (eqn (25)).

Qualitatively, the solution can be understood from a simple diagram shown in Fig. 16. A quantum vibration coupled to a transferring electron lifts the classical free energies of electron transfer by multiples of the quantum vibrational phonon $\hbar\omega_v$. There are therefore many crossing points adding to a single crossing of the standard Marcus picture. Given that $\hbar\omega_v \gg k_B T$, only the lowest state is populated on the reactants side ("1" in Fig. 16). For reactions in the normal region (Fig. 16a), these new crossings increase the barrier and quantum vibrations effectively do not change the activation energy.

The situation is significantly different in the inverted region (Fig. 16b). As before, only the ground state is populated on the reactant side, but crossings with the vibrationally excited states in the inverted region reduce the activation barrier. Vibrationally excited states carry somewhat lower weight due to the Franck-Condon overlap between the reactant and product vibrational functions thus reducing the effect of transitions involving vibrational excitations. In the normal region, the rate is multiplied with the exponential factor $\exp[-S]$, where $S = \lambda_v/(\hbar\omega_v)$ is the Huang-Rhys factor given as the ratio of the vibrational reorganization energy λ_v and the energy of the vibrational quantum $\hbar\omega_v$. The Huang-Rhys factor S carries the physical meaning of the number of vibrational excitation produced in the vertical Franck-Condon transition corresponding to the maximum of the optical absorption line.

The Franck-Condon vibrational overlap only lowers the forward rate by $\exp[-S]$ in the normal region (marked by red arrows in Fig. 17), but strongly affects the decay of the rate with increasing driving force in the inverted region. The overall energy gap law (Fig. 17) for the forward reaction is given by the Bixon-Jortner equation[27]

$$k_{ET} \propto V(R)^2 e^{-S} \sum_{m=0}^{\infty} \frac{S^m}{m!} \exp\left[-\beta \frac{(X_1 + m\hbar\omega_v)^2}{4\lambda}\right], \qquad (57)$$

where the last term comes from the Gaussian distribution function broadening and shifting each vibronic transition by the solvent modes characterized by the average energy gap $X_1 = \Delta F_0 + \lambda^{St}$ and the variance σ_1^2 given by eqn (13). m vibrational quanta added to the average energy gap increase the activation barrier in the normal region ($X_1 > 0$) and decrease it in the inverted region ($X_1 < 0$). Further, $V(R)$ is the electronic coupling between the donor and acceptor exponentially decaying with the donor-acceptor distance R. Each vibronic excitation comes with the Poisson distribution weighting factor characterized by $\langle m \rangle = S$. The Poisson weights make the overall rate constant decay with increasing driving force in the inverted region, but much slower than predicted by the classical Marcus picture (Fig. 17). This slower decay is responsible for the constraint imposed on the vibrational reorganization energy of natural photosynthesis shown in Fig. 2.

A new extension of the traditional formalism accounting for the vibronic envelope[4, 26, 27, 78, 122] appears when the promoting vi-

View Article Online
DOI: 10.1039/D2CP06072H

brational mode modulates the donor-acceptor distance R and the electronic coupling $V(R)$

$$V(R) = V_e e^{-\frac{1}{2}\gamma\delta R}. \tag{58}$$

Here, V_e is the electronic coupling at the equilibrium donor-acceptor separation, γ is the distance decay parameter, and the displacement from equilibrium $q = \delta R$ is viewed as a quantum mode to which the reorganization energy λ_v and the frequency ω_v are assigned. The model can be extended to multiple vibrational modes when $q = \delta R$ becomes one of the modes in the vibrational manifold.[27]

The vibrational reorganization energy $\lambda_v = \frac{1}{2}\kappa_v \Delta R_e^2$ is related to the alteration ΔR_e of the equilibrium distance of the vibrating bond characterized by the harmonic force constant κ_v. The equilibrium displacement $\Delta q = \Delta R_e$ defines the new parameter of the theory $\bar{\gamma} = \gamma|\Delta R_e|/(4\sqrt{S})$ which enters the modified Bixon-Jortner equation[124]

$$k_{\rm ET} \propto V_e^2 e^{-S-2\sqrt{S}\bar{\gamma}} \sum_{m=0}^{\infty} \frac{(\sqrt{S}+\bar{\gamma})^{2m}}{m!} \exp\left[-\beta\frac{(X_1+m\hbar\omega_v)^2}{4\lambda}\right]. \tag{59}$$

This equation converges to the standard result in eqn (57) at $S \gg \bar{\gamma}^2$. The new model parameter $\bar{\gamma}$ can significantly modify the energy gap law if its value is sufficiently large (green and blue lines in Fig. 17). This, however, is more likely to happen for proton and hydrogen atom transfer[125–127] because of the faster distance decay of the vibrational wave functions for more massive protons yielding $\gamma = 45 - 60$ Å^{-1}. With $\gamma = 60$ Å^{-1}, one gets $\bar{\gamma} \simeq 1.5$ at $\Delta R_e \simeq 0.1$ Å. With this estimate, $\bar{\gamma}^2$ exceeds the Huang-Rhys factor $S \simeq 1$ in the power series over the vibronic transitions in eqn (59). Such large values of $\bar{\gamma}$ strongly affect the energy-gap law: the maximum of the distorted inverted parabola shifts to much higher values of the driving force (Fig. 17). These estimates suggest that $\bar{\gamma} > 1$ makes reaching the inverted region mostly impractical. The existence of the inverted region for proton transfer without the companion electron transfer[128, 129] is still debated[130, 131] and new experimental evidence is needed.

The formalism incorporating the donor-acceptor vibration into the Franck-Condon factor allows an extension to nonequilibrium vibrational populations which can be experimentally reached by exposing the molecule to sufficiently intense continuous IR radiation or to IR pulses with duration exceeding the rate of vibrational relaxation.[132] The limit of classical vibrations affected by IR pumping is illustrative since it conceptually connects to protein electron transfer. The rate constant of electron transfer becomes proportional in this limit to the Boltzmann activation factor connecting to eqn (19)

$$k_{\rm ET} \propto \exp\left[-\beta\frac{X_1^2}{4\lambda_{\rm eff}}\right]. \tag{60}$$

Vibrations of the donor-acceptor distance lead to an effective variance reorganization energy $\lambda_{\rm eff}$ given by

$$\lambda_{\rm eff} = \lambda + \beta(\hbar\omega_v)^2 \bar{n}(S+\bar{\gamma}^2), \tag{61}$$

where $\bar{n}$ is the stationary nonequilibrium population of the donor-acceptor vibrational mode. It becomes equal to $\bar{n} = \bar{n}_{\rm eq} = (\beta\hbar\omega_v)^{-1}$ in the equilibrium limit of classical vibrations. From this solution, one anticipates an exponential enhancement of the electron-transfer rate with increasing nonequilibrium population $\Delta n = \bar{n} - \bar{n}_{\rm eq}$ of the donor-acceptor bond

$$\frac{k_{\rm ET}(\bar{n})}{k_{\rm ET}(\bar{n}_{\rm eq})} = \exp[A\Delta n], \tag{62}$$

where the second term in $\lambda_{\rm eff}$ in eqn (61) was assumed to be small compared λ and the constant $A > 0$ incorporates the rest of activation parameters. The transition rate is therefore enhanced when a nonequilibrium population of donor-acceptor vibrations is produced by IR pumping.[132–134]

Similarly to phenomenology found for protein electron transfer (eqn (49)), eqn (60) offers a separation between the Stokes-shift and variance reorganization energies, $\lambda_{\rm eff} > \lambda^{\rm St}$. Even if the standard Marcus prescription $\lambda^{\rm St} = \lambda$ is maintained for the solvent mode coupled to electron transfer, a nonequilibrium population of the donor-acceptor and other vibrations[124] leads to the breakdown of this relation. Nonequilibrium phenomena, which can be modeled by imposed constraints (Fig. 14), thus universally induce separation of $\lambda^{\rm St}$ and λ. We now discuss similar phenomenology found for electron transfer in nonpolar solvents.

7 From polar to nonpolar solvents

A significant class of electron-transfer reactions where prescriptions of standard theories are expected to break down is electron transfer in nonpolar media.[135–137] Nonpolar solvents are composed of molecules with both molecular dipole and quadrupole moments sufficiently close to zero to produce small reorganization energy. These media present a limiting case for which the standard models[6] offer no physical mechanism for electron transfer. Classical theories predict the solvent reorganization energy to scale linearly with the Pekar factor[59] (eqn (35)). Accordingly, the reorganization energy is expected to drop to a nearly zero value when the static dielectric constant ε_s approaches $\varepsilon_\infty \simeq n_D^2$ in nonpolar solvents, where n_D is the solvent refractive index. In contrast to this prediction, quite substantial reorganization energies in nonpolar solvents have been reported experimentally.[138–142]

The standard models view fluctuations of quantum energy states as produced by Coulomb interactions of the electron with the solvent permanent dipoles (eqn (32)). In the absence of permanent dipoles and of corresponding dipolar rotations, one needs to define alternative nuclear fluctuations shifting electronic states to the tunneling configuration $X = 0$. Physical interactions allowing such fluctuations are also electrostatic in character. However, instead of interactions with permanent dipoles, the interaction of the electron is with induced dipoles, via the induction forces.[143] The nuclear fluctuations are afforded not by dipolar rotations, but, instead, by translations of the induced dipole, i.e., through

View Article Online
DOI: 10.1039/D2CP06072H

density fluctuations.

To be more specific, one can consider electrostatics applicable to studies of intramolecular optical charge-transfer bands.[142] The solute is viewed as a dipolar particle changing its dipole moment with charge transfer from $\mathbf{m}_1$ in the initial state to $\mathbf{m}_2$ in the final charge-transfer state; $\Delta\mathbf{m} = \mathbf{m}_2 - \mathbf{m}_1$ is the change of the molecular dipole (Fig. 10). The induction interaction between the solute dipole and polarizable solvent molecules is proportional to the molecular polarizability α and scales with the distance as r^{-6}

$$F_{ei} = -m_i^2 U, \quad U = \sum_j v(j). \tag{63}$$

Here, the interaction potential energy is

$$v(j) = (\alpha/r_j^6)\left[1 + P_2(\hat{\mathbf{m}}\cdot\hat{\mathbf{r}}_j)\right] \tag{64}$$

and $P_2(x)$ is the second-order Legendre polynomial between the unit vector of the solute dipole $\hat{\mathbf{m}} = \mathbf{m}/m$ and the position of molecule j in the solvent $\hat{\mathbf{r}}_j = \mathbf{r}_j/r_j$. Correspondingly, $\Delta v(j)$ in eqn (32) is replaced with

$$\Delta v(j) = -\delta m^2 v(j), \tag{65}$$

where $\delta m^2 = m_2^2 - m_1^2$. The solvent-induced component of the energy gap becomes $X_s = F_{e2} - F_{e1}$ yielding the Stokes-shift reorganization energy as follows

$$2\lambda^{\mathrm{St}} = \delta m^2\left[\langle U\rangle_2 - \langle U\rangle_1\right]. \tag{66}$$

The variance reorganization energy is found from the variance of the interaction potential (eqn (1))

$$\lambda = \tfrac{1}{2}\beta(\delta m^2)^2\langle(\delta U)^2\rangle, \tag{67}$$

where the fluctuating solute-solvent interaction energy U is a sum of all individual interaction energies (eqn (63)).

The next steps follow the procedures outlined above for polar liquids (eqn (31)), except that one has to introduce the microscopic density response of the molecular liquid to describe density fluctuations. This goal is achieved[143] through the density-density structure factor[43] $S(k)$ specifying the variance of the interaction potential due to molecular translations

$$\langle(\delta U)^2\rangle = \rho\int\frac{d\mathbf{k}}{(2\pi)^3}\tilde{v}(\mathbf{k})^2 S(k). \tag{68}$$

The density structure factor, experimentally determined by scattering techniques,[144, 145] is specified in reciprocal space and, therefore, $\tilde{v}(\mathbf{k})$ in eqn (68) is the spatial Fourier transform of the real-space interaction energy in eqn (64). Given that interactions of the solute dipole with induced dipoles (induction interactions) decay with distance much faster, $\propto r^{-6}$, compared to to the dipole-dipole interaction, r^{-3}, one anticipates that there will be fewer solvent molecules within the interaction range and the rules of Gaussian statistics imposed by the central limit theorem might be violated. This indeed follows from the analysis of absorption and emission band-shapes of the DCVA chromophore[98, 99] (Fig. 10) in cyclohexane.

The results of global band-fitting analysis of DCVA at a number of temperatures are shown in Fig. 18. The analysis provides two variance reorganization energies λ_i (eqn (14)) and the Stokes-shift reorganization energy λ^{St} (eqn (17)). One finds substantial values for the variance reorganization energies, $\lambda_1 \simeq 0.17$ and $\lambda_2 \simeq 0.47$ eV. In addition, λ^{St} falls between λ_1 and λ_2, in agreement with prescriptions of the Q-model (eqn (44)). A part of the reorganization energies shown in Fig. 18 can be assigned to classical intramolecular vibrations and only $\lambda^{\mathrm{St}} \simeq 0.14$ eV was estimated to arise from the cyclohexane solvent. Similar values of the solvent reorganization energy were previously reported for molecular systems[138, 140] and, more recently, for semiconductor nanoparticles dissolved in alkanes.[141]

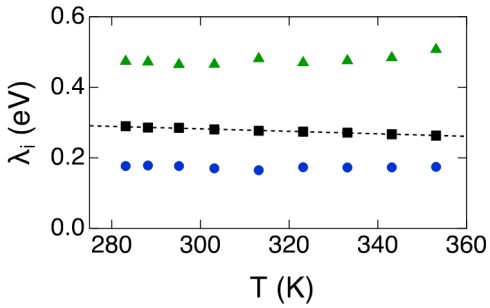

Fig. 18 Variance reorganization energies for absorption (blue) and emission (green) transitions and λ^{St} (black) vs T.[142] The results are from the band-shape analysis for the DCVA chromophore[98, 99] (Fig. 10). The dashed line is drawn through the Stokes-shift data.

The results for electron transfer in nonpolar solvents strongly deviate from predictions of standard models, but are, in many ways, similar to phenomenology found for redox-active proteins. Protein phenomenology is related to the violation of sampling rules prescribed by the Gibbsian statistics. The situation is somewhat different with electron transfer in nonpolar solvents. Violations of the standard theory arise from the microscopic nature of the solute-solvent interaction (eqn (63) and (64)). Due to its short range, fluctuations of the energy gap do not follow the statistical rules derived for macroscopic and quasi-macroscopic collective coordinates. The resulting phenomenology of FDT violation turns out to be similar in very different physical systems: one universally finds separation of the Stokes-shift and variance reorganization energies.

8 Discussion

Marcus theory of electron transfer[6] is a time-proven framework for understanding radiationless and photoinduced electronic transitions in molecules. It rests on several fundamental assumptions: (1) The Gaussian statistics of the medium fluctuations, (2) The fluctuation-dissipation (Johnson-Nyquist[40]) linear scaling of the Gaussian variance with temperature, (3) The linear coupling of the quantum subsystem to the medium coordinates, and (4) The Gibbsian statistics for the medium configurations affecting the quantum subsystem. These assumptions impose a number of bottlenecks on the energetics of electron transport in charge-transfer chains made of molecules. The main practical restriction impacting harvesting of light energy is the con-

View Article Online
DOI: 10.1039/D2CP06072H

dition of the driving force matching the reorganization energy at the maximum transition rate. The driving force at the rate maximum is reduced through either a lower reorganization energy or by stepping beyond the linear Marcusian framework.

The Gaussian statistics is likely the most robust part of the theory: it is the consequence of the long range of electrostatic interactions involving many molecules within the interaction distance. It is, therefore, a consequence of the central limit theorem, that is the law of large numbers. The interaction potential becomes more short-ranged in nonpolar liquids, when the electron-dipole interaction in a polar liquid is replaced with the electron-induced dipole interaction in a nonpolar liquid. These media are increasingly used in applications to solar energy conversion because of low reorganization energy penalties involved.[146, 147]

Electron transfer in nonpolar solvents challenges yet another assumption of standard theories: the linear scaling of the energy gap variance σ_i^2 (eqn (13)) with temperature (Johnson-Nyquist noise[40]). This anticipated scaling allows one to define the variance reorganization energy (eqn (1)) as a meaningful parameter weakly affected by temperature. The linear temperature scaling strictly applies to the variance $\langle(\delta A)^2\rangle \propto T$ of a macroscopic variable A and might become less accurate on the microscopic length scale. It holds well for long-ranged electron-dipole interactions modulated by thermally fluctuating dipolar orientations. Reorienting liquid dipoles requires an enthalpic penalty, from which the temperature scaling follows.[148] In contrast, density fluctuations rearrange close packing of molecular cores and are entropic in nature. A corresponding variance of the energy gap is nearly temperature-independent and components of the reorganization energy arising from density fluctuations gain an explicit T^{-1} dependence on temperature. This temperature scaling leads to a bell-shaped Arrhenius law shown in Fig. 6.

Marcus description of charge transfer falls under a broader umbrella of linear response theories when the source of perturbation, transferring electron in this case, can be represented by a perturbation term in the Hamiltonian being a linear function of the medium coordinates.[43] The Gaussian statistics of the thermal bath is then projected on the Gaussian statistics of the energy gap. Correspondingly, a nonlinear medium-electron coupling projects a Gaussian medium on non-Gaussian energy-gap statistics. This notion opens the door to the world on nonlinear phenomenology of charge transfer with non-parabolic free energy surfaces. Quoting from Yuen-Ron Shen:[149] "nonlinearity provides excitement in physics". It also provides an opportunity for a less generic description and leads to non-trivial phenomena. Formulation of consistent nonlinear models for charge transfer quickly becomes a challenging goal. With the steep rise of theoretical difficulty, one wonders what is the payoff. Are there any advantages to the efficiency of charge transfer that can be gained if a nonlinear scenario replaces the standard linear model?

This general question is far from being answered since very few models allow consistent analytical solutions satisfying the fundamental constraints, such as the linear relation in eqn (10). Like the Marcus model, the Q-model provides a mathematically exact analytical framework to study electron transfer. It converts to Marcus model when the force constant of medium fluctuations

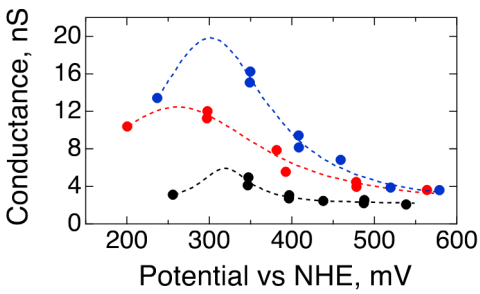

Fig. 19 Conduction resonances in streptavidin (blue), DNA polymerase Φ29 (red), and Anti-DNT (black) proteins vs the electron injection potential on the NHE scale.[151] The resonances located at ∼ 300 mV are shifted by ∼ 700 mV from the oxidation potentials of tyrosine (1.0 V[152]) and tryptophan (between 0.952 V[152] and 1.3 V vs NHE[153, 154]). The dashed lines are Lorentzian fits through the experimental points. Adapted with permission from Ref. [151].

becomes unaffected by electronic transition ($\kappa_1 = \kappa_2$). This nonlinear model shows that the energetic requirement for reaching the maximum electron-transfer rate can be softened. Marcus theory gives maximum rate at the driving force equal to the reorganization energy, while it is always lower in the Q-model (eqn (46) and Fig. 9).

Biological macromolecules, and most notably proteins, offer a much wider spectrum of possibilities for affecting electronic transitions. Proteins possess a complex hierarchy of molecular motions occurring on a broad range of characteristic time scales.[150] Most of biologically significant charge-transfer reactions fall in the range of reaction times within the protein relaxation spectrum (Fig. 4). Some of the protein motions become nearly universally frozen on the reaction time. One is forced to introduce the concept of nonergodic reorganization energy and of the corresponding nonergodic reaction barrier. Ergodicity breaking violates the Gibbsian statistics of sampling the configuration space, which is phenomenologically reflected in the separation between the Stokes-shift and variance reorganization energies (eqn (49)).

Proteins provide a complex environment in which fluctuations of the protein core, hydration water, and a small number of water molecules hydrating the protein active site produce a complex spectrum of energy-gap fluctuations with many relaxation times involved.[155] The combination of slow and fast relaxation times leading to highly dispersive dynamics can be achieved in other media, and ionic liquids provide an example of a medium mimicking protein electron transfer (Fig. 11). The set of tools to control rates of reactions and parameters to tune to affect reactivity clearly increases. The picture of nonergodic electron transfer makes the relaxation time, in addition to thermodynamic driving forces, a new parameter to tune the reaction rate.

This article is mostly about the reorganization energy of electron transfer, but the reaction free energy takes an equally important position in electron-transfer theories and its alteration is responsible for the inverted bell-shaped parabola (Fig. 17) and the inverted region of electron transfer. The reduction of the reaction free energy due to nonergodic sampling from the thermodynamic value ΔF_0 to its nonergodic counterpart $\Delta F_0'$ (eqn (52)) can signif-

View Article Online
DOI: 10.1039/D2CP06072H

icantly affect the role of driving force in biological charge transport. It might explain the empirical observation of little sensitivity of charge-transport chains to changes of redox potential[156] and the observation of uphill, in free energy, electron hops in biological energy chains.[157, 158]

A confirmation of nonergodic character of the driving force in proteins has arrived from single-molecule electrochemical scanning tunneling microscopy measurements.[151, 159, 160] Electron injection into proteins was studied by combining gold, palladium and platinum electrodes, along with varying the substrate potential in a single-protein junction (Fig. 19). Resonance in conductance vs the electrode potential indicates that electrons are injected into localized states within the protein likely to be associated with aromatic amino acids.[154] However, the conductance resonances are shifted by $\simeq 0.7$ V from the nearest equilibrium oxidation potentials of tryptophan (between 0.952 V[152] and 1.3 V[153, 154] for radical cation formation) and of tyrosine (1.0 V for the neutral phenol radical[152]). The shift is consistent with eqn (52) when $\lambda^{St}/\lambda \sim 0.3$, often found in protein electron transfer,[103] is adopted.

The field of electron transfer is actively moving toward mesoscopic systems of charge transport, including biological nanowires made of polymerized redox-active proteins (cytochromes).[161, 162] Long-ranged conductivity through amino acid relays[151, 154, 163] adds versatility to the pathways by which charge can traverse mesoscopic distances in biology. The more traditional mechanism of interprotein charge transfer is still insufficiently understood because of high computational resources required for simulations and difficulty of controlling the kinetics in the laboratory setting. Whether the nonergodic mechanism of lowering the activation barrier applies to these reactions remains an open question.

The difficulty of assigning reorganization energy to interprotein electron transport goes back to early attempts to fit classical DeVault and Chance experiments for charge transfer between cytochromes and bacterial reaction centers,[164] which resulted in quite high, 2.24[165] and 2.10 eV,[166] medium reorganization energies.[15] These uncertainties have never been resolved. For instance, recent measurements of electron transport in crystalline lattices of tetraheme chromophores have shown very slow hopping rates requiring reorganization energies in the range $1.14 - 1.82$ eV.[158] Electrochemistry of proteins, on the other hand, suggests that half redox reactions of proteins immobilized on metal electrodes have very low reorganization energies in the range $0.15 - 0.2$ eV.[107] This seems to become possible because of a partial dehydration of a globular protein when attached to organic surface layers covering the electrode.[115] The hydration water is partially removed and the nonergodic statistics of the protein (Fig. 12) becomes effective in lowering the activation energy. This mechanism might explain the performance of electron shuttle proteins (plastocyanins, azurins, ferredoxins, and cytochromes) in biological energy chains: the reaction is allowed upon binding to a large protein complex.

The potential range of reorganization energy values is quite broad. It might carry biological significance since, along with the need to transport electrons by small electron shuttles, more general considerations suggest that controlling the rate of oxidative phosphorylation in respiratory chains requires stopping cross-membrane electron transport when needed. A dramatic example of this biological necessity is the ability of periplasm cytochromes of microbes to act as electron capacitors to store electrons during the periods when extracellular electron acceptors become unavailable.[167] Reverse reactions must be quite slow for this mechanism to operate.

9 Outlook

Efficient transport of charge through molecules in natural and artificial photosynthesis requires low values of the medium reorganization energy for charge transfer. Analyzing mechanisms allowing such conditions have broadened our understanding of the meaning of an ensemble average when applied to systems with dispersive dynamics (proteins, ionic liquids, etc). The main fundamental result is that dynamics and separation of time scales affect statistically averaged quantities making them deviate from the corresponding equilibrium thermodynamic parameters. The question of whether this rule applies to enzymatic reactions in general and can provide mechanisms for lowering activation barriers in biology remains a challenge for future studies.

Conflicts of interest

There are no conflicts to declare.

Acknowledgements

This research was supported by the National Science Foundation (CHE-2154465).

Notes and references

1 R. A. Marcus, *J. Chem. Phys.*, 1956, **24**, 979–989.
2 R. A. Marcus, *J. Chem. Phys.*, 1963, **39**, 1734–1740.
3 A. Nitzan, *Chemical Dynamics in Condensed Phases: Relaxation, Transfer and Reactions in Condensed Molecular Systems*, Oxford University Press, Oxford, 2006.
4 M. Lax, *J. Chem. Phys.*, 1952, **20**, 1752–1760.
5 A. Warshel, *J. Phys. Chem.*, 1982, **86**, 2218–2224.
6 R. A. Marcus and N. Sutin, *Biochim. Biophys. Acta*, 1985, **811**, 265–322.
7 P. F. Barbara, T. J. Meyer and M. A. Ratner, *J. Phys. Chem.*, 1996, **100**, 13148–13168.
8 J. Ulstrup, *Charge Transfer Processes in Condensed Media*, Springer-Verlag, Berlin, 1979.
9 A. J. Hoff and J. Deisenhofer, *Phys. Rep.*, 1997, **287**, 1–247.
10 R. E. Blankenship, D. M. Tiede, J. Barber, G. W. Brudvig, G. Fleming, M. Ghirardi, M. R. Gunner, W. Junge, D. M. Kramer, A. Melis, T. A. Moore, C. C. Moser, D. G. Nocera, A. J. Nozik, D. R. Ort, W. W. Parson, R. C. Prince and R. T. Sayre, *Science*, 2011, **332**, 805 – 809.
11 J. H. Alstrum-Acevedo, M. K. Brennaman and T. J. Meyer, *Inorg. Chem.*, 2005, **44**, 6802.
12 F. E. Osterloh, *ACS Energy Letters*, 2017, **2**, 445–453.
13 D. Gust, T. A. Moore and A. L. Moore, *Acc. Chem. Res.*, 2009, **42**, 1890–1898.

View Article Online
DOI: 10.1039/D2CP06072H

14 D. M. Guldi, *Phys. Chem. Chem. Phys.*, 2007, **9**, 1400.
15 D. DeVault, *Quantum-Mechanical Tunneling in Biologycal Systems*, Cambridge University Press, Cambridge, UK, 1984.
16 R. E. Blankenship, *Molecular Mechanisms of Photosynthesis*, Blackwell Science, Williston, VT, 2003.
17 H. Wang, S. Lin, J. P. Allen, J. C. Williams, S. Blankert, C. Laser and N. W. Woodbury, *Science*, 2007, **316**, 747–750.
18 D. N. LeBard, V. Kapko and D. V. Matyushov, *J. Phys. Chem. B*, 2008, **112**, 10322–10342.
19 D. N. LeBard, D. R. Martin, S. Lin, N. W. Woodbury and D. V. Matyushov, *Chem. Sci.*, 2013, **4**, 4127—4136.
20 L. Laporte, C. Kirmaier, C. C. Schenck and D. Holten, *Chem. Phys.*, 1995, **97**, 225–237.
21 R. A. Marcus, *Electron transfer reactions in chemistry: Theory and experiment. Nobel lecture in chemistry*, 1992.
22 D. J. Barlow and J. M. Thornton, *Biopolymers*, 1986, **25**, 1717–1733.
23 D. N. LeBard and D. V. Matyushov, *Phys. Chem. Chem. Phys.*, 2010, **12**, 15335–15348.
24 C. C. Page, C. C. Moser, X. X. Chen and P. L. Dutton, *Nature*, 1999, **402**, 47–52.
25 D. G. Nicholls and S. J. Ferguson, *Bioenergetics4*, Academic Press, Amsterdam, 2013.
26 K. Huang and A. Rhys, *Proc. R. Soc. London Ser. A*, 1950, **204**, 406–423.
27 M. Bixon and J. Jortner, *Adv. Chem. Phys.*, 1999, **106**, 35–202.
28 E. Sigfriddson, M. H. M. Olsson and U. Ryde, *J. Phys. Chem. B*, 2001, **105**, 5546–5552.
29 X. Amashukeli, N. E. Gruhn, D. L. Lichtenberger, J. R. Winkler and H. B. Gray, *J. Am. Chem. Soc.*, 2004, **126**, 15566–15571.
30 M. Cascella, A. Magistrato, I. Tavernelli, P. Carloni and U. Rothlisberger, *Proc. Natl. Acad. Sci.*, 2006, **103**, 19641–19646.
31 A. J. Bard and L. R. Faulkner, *Electrochemical Methods. Fundamentals and Applications*, Wiley, New York, 2nd edn., 2001.
32 D. V. Matyushov, *J. Phys.: Condens. Matter*, 2015, **27**, 473001.
33 C. H. Bennett, *J. Comput. Phys.*, 1976, **22**, 245–268.
34 M. Tachiya, *J. Phys. Chem.*, 1989, **93**, 7050–7052.
35 P. Chen and T. J. Meyer, *Chem. Rev.*, 1998, **98**, 1439.
36 D. V. Matyushov and M. D. Newton, *J. Phys. Chem. B*, 2018, **122**, 12302–12311.
37 R. A. Marcus and N. Sutin, *Comments on Inorg. Chem.*, 1986, **5**, 119–133.
38 J. R. Miller, L. T. Calcaterra and G. L. Closs, *J. Am. Chem. Soc.*, 1984, **106**, 3047–3049.
39 M. R. Wasielewski, M. P. Niemczyk, W. Svec and E. B. Pewitt, *J. Am. Chem. Soc*, 1985, **107**, 1080–1083.
40 R. P. Feynman, R. B. Leighton and M. Sands, *The Feynman lectures on physics, Vol. I: Mainly mechanics, radiation, and heat*, Addison-Wesley, Reading, MA, 1963.
41 G. van der Zwan and J. T. Hynes, *J. Phys. Chem.*, 1985, **89**, 4181–4188.
42 R. Kubo, in *Lectures in Theoretical Physics*, Interscience Publishers, Inc., New York, 1959, vol. 1, p. 120.
43 J.-P. Hansen and I. R. McDonald, *Theory of Simple Liquids*, Academic Press, Amsterdam, 4th edn., 2013.
44 B. J. Berne and R. Pecora, *Dynamic Light Scattering*, Dover Publications, Inc., Mineola, N.Y., 2000.
45 R. Zwanzig, *Nonequilibrium Statistical Mechanics*, Oxford University Press, Oxford, 2001.
46 M. Maroncelli, *J. Mol. Liq.*, 1993, **57**, 1–37.
47 M. Maroncelli and G. R. Fleming, *J. Chem. Phys.*, 1988, **89**, 5044–5069.
48 E. A. Carter and J. T. Hynes, *J. Chem. Phys.*, 1991, **94**, 5961.
49 V. May and O. Kühn, *Charge and Energy Transfer Dynamics in Molecular Systems*, Wiley-VCH, Berlin, 3rd edn., 2011.
50 S. Mukamel, *Principles of Nonlinear Optical Spectroscopy*, Oxford University Press, New York, 1995.
51 C. G. Gray and K. E. Gubbins, *Theory of Molecular Liquids*, Clarendon Press, Oxford, 1984, vol. 1: Fundamentals.
52 D. V. Matyushov, *Mol. Phys.*, 1993, **79**, 795.
53 P. K. Ghorai and D. V. Matyushov, *J. Phys. Chem. B*, 2020, **124**, 3754–3769.
54 R. Richert and D. V. Matyushov, *J. Phys.: Condens. Matter*, 2021, **33**, 385101.
55 T. Fonseca and B. M. Ladanyi, *J. Chem. Phys.*, 1990, **93**, 8148–8155.
56 D. V. Matyushov, *J. Chem. Phys.*, 2004, **120**, 7532–7556.
57 O. V. Dolgov, D. A. Kirzhnits and E. G. Maksimov, *Rev. Mod. Phys.*, 1981, **53**, 81–93.
58 P. A. Bopp, A. A. Kornyshev and G. Sutmann, *Phys. Rev. Lett.*, 1996, **76**, 1280.
59 S. I. Pekar, *Research in electron theory of crystals*, USAEC, Washington, D.C., 1963.
60 R. P. Feynman, *Phys. Rev.*, 1955, **97**, 660.
61 P. Vath, M. B. Zimmt, D. V. Matyushov and G. A. Voth, *J. Phys. Chem. B*, 1999, **103**, 9130–9140.
62 M. M. Waskasi, G. Kodis, A. L. Moore, T. A. Moore, D. Gust and D. V. Matyushov, *J. Am. Chem. Soc.*, 2016, **138**, 9251–9257.
63 D. Gust, T. A. Moore and A. L. Moore, *Acc. Chem. Res.*, 1993, **26**, 198.
64 C. S. Santos, N. S. Murthy, G. A. Baker and E. W. Castner Jr, *J. Chem. Phys.*, 2011, **134**, 121101–5.
65 J. C. Araque, J. J. Hettige and C. J. Margulis, *J. Phys. Chem. B*, 2015, **119**, 12727–12740.
66 J. G. McDaniel and A. Yethiraj, *J. Phys. Chem. B*, 2019, **123**, 3499–3512.
67 S. Seyedi, D. R. Martin and D. V. Matyushov, *J. Phys.: Condense Matter*, 2019, **31**, 325101.
68 M. Dinpajooh, M. D. Newton and D. V. Matyushov, *J. Chem. Phys.*, 2017, **146**, 064504.
69 G. Stell, G. N. Patey and J. S. Høye, *Adv. Chem. Phys.*, 1981, **48**, 183–328.
70 H. Fröhlich, *Theory of Dielectrics*, Oxford University Press, Oxford, 1958.
71 D. V. Matyushov, *Chem. Phys.*, 1993, **174**, 199–218.
72 C. J. F. Böttcher, *Theory of Electric Polarization, Vol. 1: Dielectrics*

View Article Online
DOI: 10.1039/D2CP06072H

in Static Fields, Elsevier, Amsterdam, 1973.
73 J. S. Bader and B. J. Berne, *J. Chem. Phys.*, 1996, **104**, 1293.
74 S. Gupta and D. V. Matyushov, *J. Phys. Chem. A*, 2004, **108**, 2087–2096.
75 G. Lüdemann, P. B. Woiczikowski, T. Kubař, M. Elstner and T. B. Steinbrecher, *J. Phys. Chem. B*, 2013, **117**, 10769–10778.
76 C. C. Page, C. C. Moser and P. L. Dutton, *Curr. Opinion in Biology*, 2003, **7**, 551.
77 Y. Eshel, U. Peskin and N. Amdursky, *Nanotechnology*, 2020, **31**, 314002.
78 R. Kubo and Y. Toyozawa, *Prog. Theor. Phys.*, 1955, **13**, 160.
79 D. V. Matyushov and M. D. Newton, *Phys. Chem. Chem. Phys.*, 2018, **20**, 24176–24185.
80 G. Fischer, *Vibronic Coupling*, Academic Press, London, 1984.
81 D. V. Matyushov and G. A. Voth, *J. Chem. Phys.*, 2000, **113**, 5413.
82 S. M. Sarhangi and D. V. Matyushov, *J. Phys. Chem. B*, 2022, 10.26434/chemrxiv–2022–fnfck.
83 C. Hartnig and M. T. M. Koper, *J. Chem. Phys.*, 2001, **115**, 8540.
84 H.-X. Zhou and A. Szabo, *J. Chem. Phys.*, 1995, **103**, 3481.
85 G. Hummer, L. R. Pratt, A. E. García, B. J. Berne and S. W. Rick, *J. Phys. Chem. B*, 1997, **101**, 3017–3020.
86 S. Chakrabarty and A. Warshel, *Proteins*, 2013, **81**, 93–106.
87 C. A. Bortolotti, A. Amadei, M. Aschi, M. Borsari, S. Corni, M. Sola and I. Daidone, *J. Am. Chem. Soc.*, 2012, **134**, 13670–13678.
88 D. R. Martin and D. V. Matyushov, *Sci. Rep.*, 2017, **7**, 5495.
89 M. M. Waskasi, D. R. Martin and D. V. Matyushov, *J. Phys. Chem. B*, 2018, **122**, 10490–10495.
90 S. D. E. Fried, K. S. K. Hewage, A. R. Eitel, A. V. Struts, N. Weerasinghe, S. M. D. C. Perera and M. F. Brown, *Proc. Natl. Acad. Sci. U.S.A.*, 2022, **119**, e2117349119.
91 M. M. Waskasi, M. D. Newton and D. V. Matyushov, *J. Phys. Chem. B*, 2017, **121**, 2665–2676.
92 R. G. Palmer, *Adv. Phys.*, 1982, **31**, 669–735.
93 J. M. R. Parrondo, J. M. Horowitz and T. Sagawa, *Nat. Phys.*, 2015, **11**, 131–139.
94 D. V. Matyushov, *J. Chem. Phys.*, 2009, **130**, 164522.
95 R. S. Lumpkin and T. J. Meyer, *J. Phys. Chem.*, 1986, **90**, 5307.
96 N. Ito, K. Duvvuri, D. V. Matyushov and R. Richert, *J. Chem. Phys.*, 2006, **125**, 024504.
97 G. Kodis, M. Z. Ertem, M. D. Newton and D. V. Matyushov, *J. Phys. Chem. Lett.*, 2022, **13**, 3297–3303.
98 P. Pasman, F. Rob and J. W. Verhoeven, *J. Am. Chem. Soc.*, 1982, **104**, 5127–5133.
99 T. Mukherjee, N. Ito and I. R. Gould, *J. Phys. Chem. A*, 2011, **115**, 1837–1843.
100 H. Frauenfelder, *The Physics of Proteins. An Introduction to Biological Physics and Molecular Biophysics*, Springer, New York, 2010.
101 A. Crisanti and F. Ritort, *J. Phys. A: Math. Gen.*, 2003, **36**, R181–290.
102 J. Kurchan, *Nature*, 2005, **433**, 222–225.
103 D. V. Matyushov, *J. Chem. Phys.*, 2013, **139**, 025102.
104 J. Blumberger, *Chem. Rev.*, 2015, **115**, 11191–11238.
105 H. B. Gray and J. R. Winkler, *Proc. Natl. Acad. Sci.*, 2005, **102**, 3534–3539.
106 S. Seyedi, M. M. Waskasi and D. V. Matyushov, *J. Phys. Chem. B*, 2017, **121**, 4958–4967.
107 P. Hildebrandt and D. H. Murgida, *Bioelectrochemistry*, 2002, **55**, 139–143.
108 J. J. Wei, H. Liu, K. Niki, E. Margoliash and D. H. Waldeck, *J. Phys. Chem. B*, 2004, **108**, 16912–16917.
109 D. E. Khoshtariya, T. D. Dolidze, M. Shushanyan, K. L. Davis, D. H. Waldeck and R. van Eldik, *Proc. Natl. Acad. Sci. USA*, 2010, **107**, 2757–2762.
110 S. Monari, G. Battistuzzi, C. A. Bortolotti, S. Yanagisawa, K. Sato, C. Li, I. Salard, D. Kostrz, M. Borsari, A. Ranieri, C. Dennison and M. Sola, *J. Am. Chem. Soc.*, 2012, **134**, 11848–11851.
111 U. A. Zitare, J. Szuster, M. C. Santalla, M. N. Morgada, A. J. Vila and D. H. Murgida, *Electrochim. Acta*, 2020, **342**, 136095.
112 L. D. Landau and E. M. Lifshits, *Statistical Physics*, Pergamon Press, New York, 1980.
113 D. R. Martin and D. V. Matyushov, *J. Chem. Phys.*, 2015, **142**, 161101.
114 J. Li, J. Xie, A. Godec, K. R. Weninger, C. Liu, J. C. Smith and L. Hong, *Chem. Sci.*, 2022.
115 S. M. Sarhangi and D. V. Matyushov, *J. Phys. Chem. B*, 2022, **126**, 3000–3011.
116 O. V. Kontkanen, D. Biriukov and Z. Futera, *J. Chem. Phys.*, 2022, **156**, 175101.
117 H. Reiss, *Methods of Thermodynamics*, Dover Publications, Inc., Mineola, N. Y., 1996.
118 S. Seyedi and D. V. Matyushov, *J. Phys. Chem. Lett.*, 2018, **9**, 2359–2366.
119 F. G. Parak, *Rep. Prog. Phys.*, 2003, **66**, 103–129.
120 W. Doster, *Biochim. Biophys. Acta*, 2010, **1804**, 3–14.
121 D. V. Matyushov, *J. Molec. Liq.*, 2018, **266**, 361–372.
122 A. S. Davydov, *Sov. Phys. JETP*, 1953, **24**, 397–408.
123 N. R. Kestner, J. Logan and J. Jortner, *J. Phys. Chem.*, 1974, **78**, 2148–2166.
124 D. V. Matyushov, *J. Chem. Phys.*, 2019, **150**, 074504–9.
125 D. C. Borgis, S. Lee and J. T. Hynes, *Chem. Phys. Lett.*, 1989, **162**, 19–26.
126 D. Borgis and J. Hynes, *J. Phys. Chem.*, 1996, **100**, 1118–1128.
127 E. Hatcher, A. V. Soudackov and S. Hammes-Schiffer, *J. Am. Chem. Soc.*, 2007, **129**, 187–196.
128 G. A. Parada, Z. K. Goldsmith, S. Kolmar, B. P. Rimgard, B. Q. Mercado, L. Hammarström, S. Hammes-Schiffer and J. M. Mayer, *Science*, 2019, **364**, 471–475.
129 R. Tyburski, T. Liu, S. D. Glover and L. Hammarström, *J. Am. Chem. Soc.*, 2021, **143**, 560–576.
130 K. S. Peters, *Acc. Chem. Res.*, 2009, **42**, 89–96.
131 H.-C. Chen, A. R. Cook, S. Asaoka, J. S. Boschen, T. L. Windus and J. R. Miller, *Phys. Chem. Chem. Phys.*, 2017, **19**, 32272–32285.
132 M. Delor, P. A. Scattergood, I. V. Sazanovich, A. W. Parker, G. M. Greetham, A. J. H. M. Meijer, M. Towrie and J. A. Weinstein, *Science*, 2014, **346**, 1492.
133 X. Yang, T. Keane, M. Delor, A. J. H. M. Meijer, J. Weinstein and

View Article Online
DOI: 10.1039/D2CP06072H

E. R. Bittner, *Nat. Comm.*, 2017, **8**, 14554–8.
134 S. Valianti and S. S. Skourtis, *Mol. Phys.*, 2018, **106**, 1–14.
135 D. V. Matyushov and R. Schmid, *J. Chem. Phys.*, 1995, **103**, 2034–2049.
136 D. S. Larsen, K. Ohta and G. R. Fleming, *J. Chem. Phys.*, 1999, **111**, 8970–8979.
137 I. V. Leontyev and M. Tachiya, *J. Chem. Phys.*, 2005, **123**, 224502.
138 G. L. Closs and J. R. Miller, *Science*, 1988, **240**, 440–447.
139 J. M. Chen, T. I. Ho and C. Mou, *J. Phys. Chem.*, 1990, **94**, 2889–2896.
140 R. A. Holroyd and J. R. Miller, *J. Phys. Chem. B*, 2019, **123**, 9206–9211.
141 J. Wang, T. Ding, K. Gao, L. Wang, P. Zhou and K. Wu, *Nat. Comm.*, 2021, **12**, 6333.
142 G. Kodis, I. R. Gould and D. V. Matyushov, *Phys. Rev. Res.*, 2020, **3**, 013109.
143 D. V. Matyushov, *Phys. Chem. Chem. Phys.*, 2020, **22**, 10653–10665.
144 S. W. Lovesey, *Theory of Neutron Scattering from Condensed Matter*, Clarendon Press, Oxford, 1984, vol. 1.
145 A. Furrer, J. Mesot and T. Strässel, *Neutron Scattering in Condensed Matter Physics*, World Scientific, 2009, vol. 4.
146 J. Benduhn, K. Tvingstedt, F. Piersimoni, S. Ullbrich, Y. Fan, M. Tropiano, K. A. McGarry, O. Zeika, M. K. Riede, C. J. Douglas, S. Barlow, S. R. Marder, D. Neher, D. Spoltore and K. Vandewal, *Nat. Energy*, 2017, **2**, 297–6.
147 M. Azzouzi, J. Yan, T. Kirchartz, K. Liu, J. Wang, H. Wu and J. Nelson, *Phys. Rev. X*, 2018, **8**, 031055–14.
148 P. K. Ghorai and D. V. Matyushov, *J. Phys. Chem. A*, 2006, **110**, 8857–8863.
149 Y. R. Shen, *The Principles of Nonlinear Optics*, Wiley-Interscience, New Jersey, 2003.
150 J. R. Lewandowski, M. E. Halse, M. Blackledge and L. Emsley, *Science*, 2015, **348**, 578–581.
151 S. Lindsay, *Life*, 2020, **10**, 72–13.
152 K. J. Tyson, A. N. Davis, J. L. Norris, L. J. Bartolotti, E. G. Hvastkovs and A. R. Offenbacher, *J. Phys. Chem. Lett.*, 2020, **11**, 2408–2413.
153 S. D. Glover, R. Tyburski, L. Liang, C. Tommos and L. Hammarström, *J. Am. Chem. Soc.*, 2018, **140**, 185–192.
154 H. B. Gray and J. R. Winkler, *Chem. Sci.*, 2021, **12**, 13988–14003.
155 M.-C. Bellissent-Funel, A. Hassanali, M. Havenith, R. Henchman, P. Pohl, F. Sterpone, D. van der Spoel, Y. Xu and A. E. García, *Chem. Rev.*, 2016, **116**, 7673–7697.
156 J. M. Hudson, K. Heffron, V. Kotlyar, Y. Sher, E. Maklashina, G. Cecchini and F. A. Armstrong, *J. Am. Chem. Soc*, 2005, **127**, 6977–6989.
157 C. C. Moser, C. C. Page and P. L. Dutton, *Phil. Trans. R. Soc. London B*, 2006, **361**, 1295–1305.
158 J. Huang, J. Zarzycki, M. R. Gunner, W. W. Parson, J. F. Kern, J. Yano, D. C. Ducat and D. M. Kramer, *J. Am. Chem. Soc.*, 2020, **142**, 10459–10467.
159 B. Zhang, W. Song, J. Brown, R. Nemanich and S. Lindsay, *J. Am. Chem. Soc.*, 2020, **142**, 6432–6438.
160 B. Zhang, E. Ryan, X. Wang, W. Song and S. Lindsay, *ACS Nano*, 2022, **16**, 1671–1680.
161 D. R. Lovley and D. J. F. Walker, *Frontiers in Microbiology*, 2019, **10**, 2078.
162 F. Wang, Y. Gu, J. P. O'Brien, S. M. Yi, S. E. Yalcin, V. Srikanth, C. Shen, D. Vu, N. L. Ing, A. I. Hochbaum, E. H. Egelman and N. S. Malvankar, *Cell*, 2019-04, **177**, 361–369.e10.
163 C. Shih, A. K. Museth, M. Abrahamsson, A. M. Blanco-Rodriguez, A. J. D. Bilio, J. Sudhamsu, B. R. Crane, K. L. Ronayne, M. Towrie, A. Vlček, J. H. Richards, J. R. Winkler and H. B. Gray, *Science*, 2008, **320**, 1760–1762.
164 D. de Vault and B. Chance, *Biophys. J.*, 1966, **6**, 825.
165 J. J. Hopfield, *Proc. Nat. Acad. Sci.*, 1974, **71**, 3640.
166 J. Jortner, *J. Chem. Phys.*, 1976, **64**, 4860–4867.
167 A. Esteve-Núñez, J. Sosnik, P. Visconti and D. R. Lovley, *Environmental Microbiology*, 2008, **10**, 497–505.